EXAMINATION OF THE MECHANICAL PROPERTIES OF THE REACTOR STEEL CODE 15H2NMFA

David CINGER

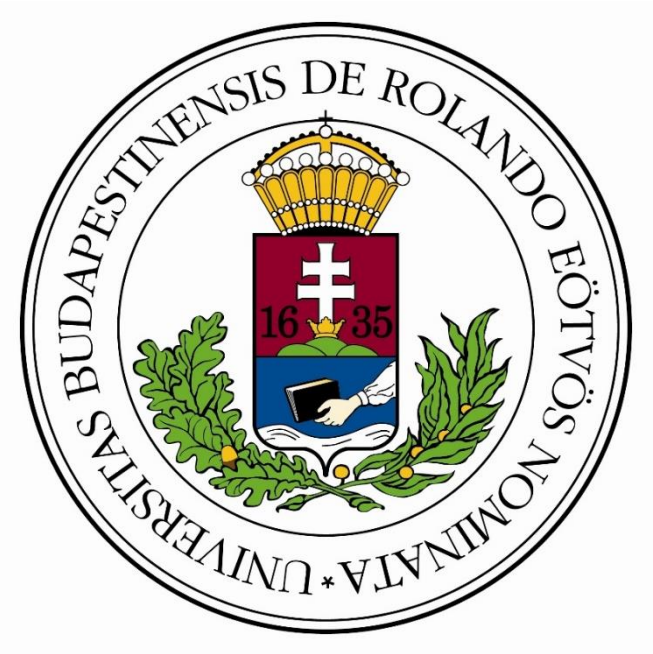

Degree program: Materials Science MSc

Supervisor: Dr. Gillemot Ferenc

Consultant: Prof. Dr. Gubicza Jenő

Budapest

2023

Abbreviations

Abreviation, definiation		*Description*
Charpy specimen		Notched standard bar for testing 10 x 10 x 55 mm
Charpy energy	Joule	Absorbed fracture energy by a Charpy specimen at impact testing
CT		Compact tension specimen
DBTT	41 Joule/cm^2	Ductile brittle transition temperature (Temperature at 41 Joule/cm^2 Charpy energy
Fracture toughness	K_{IC} or K_{JC}	Critical value of the stress intensity factor where crack propagation initialed
Stress intensity factor	MPam$^{1/2}$	Stress peak at the crack tip
Master Curve		Standard Curve describing the Fracture Toughness of ferritic-martensitic (RPV) steels in the function of temperature
PWR		Pressurized Water Reactor
Reference temperature	T_0	Temperature where the Fracture Toughness value 100 MPam$^{1/2}$
RPV		Reactor Pressure Vessel
TPB		Three point bend fracture mechanics sample

Table of contents

1. INTRODUCTION

1.1. Objective

The aim of my research is to determine the microstructural and mechanical properties of the 15H2NMFA reactor steel. On the one hand, it is important to compare the manufacturer's specifications with independent measurements, and on the other hand, to create a baseline regarding the mechanical properties of the reactor vessel. The reactors currently under construction are designed for 60-80 years of operation. It is necessary to be able to compare the measurement results of the surveillance sample sets that provide information on the damage that occurs during operation with the measurement results of the zero operating hour, so that the available data can be used to create trend curves for the lifetime of the reactor. Since 1979 the necessity of the surveillance program has been stipulated in national regulations and standards which are based on the US Federal Code 10CFR50. First of all Charpy-V and tensile test specimens have been used until now (BRYNDA ET AL., 2002). The VVER-1000 sulveillance programs were supplemented with pre-cracked Charpy fracture mechanics test specimens beyond to the Charpy-V and tensile test specimens (BRYNDA ET AL., 2003).

In addition to determining the basic mechanical properties (yield strength, tensile strength, DBTT, T_0), I performed the microstructural analysis of the material and gave an estimate of the transition temperature in the 30th and 60th service years.

1.2. Construction of a nuclear reactor

A nuclear reactor is a device used to initiate and control a fission nuclear chain reaction. In a nuclear power plant the heat produced during the controlled chain reaction is removed by the coolant and steam is produced during a multi-stage heat transfer process, which drives the power plant turbines and the generators connected to them generate electricity (Figure 1.). The reactors are mostly fueled by the isotope U-235. The U-235 nucleus splits into two or more daughter nuclei. The products of the reaction:

- kinetic energy,
- gamma radiation,
- **free neutrons**.

The released neutrons are very fast. The surrounding fissile materials are unable to contain them. Water is used to slow them down. Water thus plays a dual role in the life of PWR[1]s, moderating neutrons and functioning as a coolant. The chain reaction is controlled using control rods filled with neutron-absorbing materials (OLDEKOP, 1982).

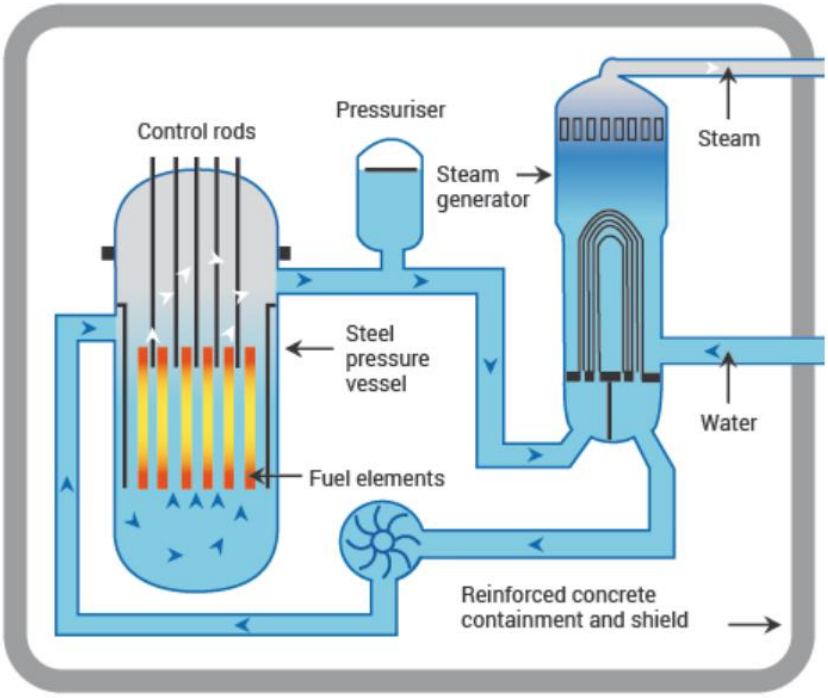

Figure 1. Schematic diagram of a nuclear power plant, *(world-nuclear.org)*

[1] Pressurized Water Reactor

1.3. VVER type reactors

The VVER (*ВВЭР – водо-водяной энергетический реактор)* is a Soviet/Russian developed pressurized water reactor family. The reactor type began to be developed in the 1950s. Its first type, a VVER-210 type, was put into operation in Novovoronyezs in 1964. Based on operational experience, the VVER-440 reactor type was created, four of which are currently in operation at the Paks nuclear power plant. At the beginning of the 70s, the VVER-1000 type appeared, the first of which was installed in block number 5 of Novovoronyezs (NOVOREFTOV, 2010).

The 15H2NMFA steel type was used for the VVER-1000 reactors for the first time, and according to the plans, it will also be used for the VVER-1200 types. Figure 2. shows the structure of the vver-1000 reactor vessel. The production of tanks begins with the casting of hundreds of tons of ingots. Steel treated in argon-flushing cauldrons under vacuum to minimize the formation of gas inclusions. The pieces are then forged into rings and then the pieces are welded together (TIMOFEEV & KARZOV, 2006).

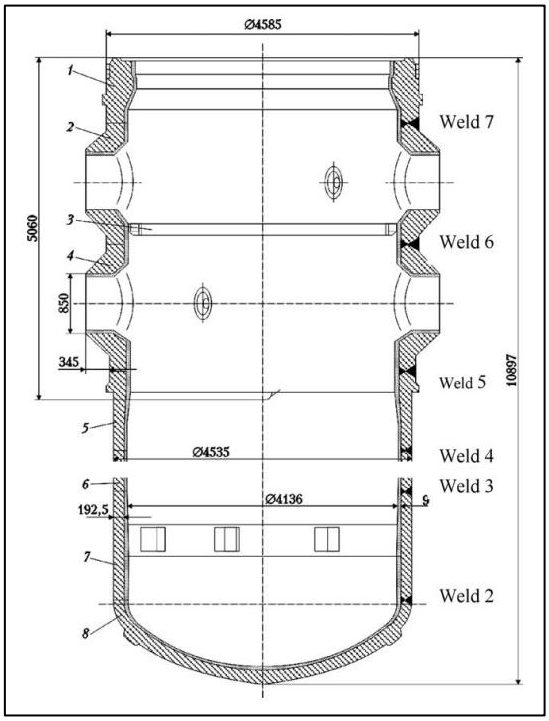

Figure 2. Drawing of the VVER-1000 reactor (TIMOFEEV & KARZOV, 2006)

It can be clearly seen that the most critical part of the reactor in terms of radiation damage and thermal aging is the core zone and weld 3 and 4.

2. 15H2NMFA REACTOR STEEL

The 15H2NMFA / 15Cr2NiMoVA / 15Х2НМФА reactor pressure vessel steel is a low alloyed ferritic-pearlitic steel with low carbon content. The requirement for the chemical composition is in table 1. (TIMOFEEV & KARZOV, 2006).

Alloying elements (balance to Fe)						
C	Si	Mn	Cr	Ni	Mo	V
0.13-0.18	0.17-0.37	0.30-0.60	1.70-2.40	1.00-1.15	0.50-0.70	<0.12
Other elements (not more than)						
Cu	S	P	As	Co		
0.30	0.02	0.020	0.04	0.03		

Table 1. Chemical composition of 15H2NMFA steel (TIMOFEEV & KARZOV, 2006)

15H2NMFA is not an entirely new type. Cr-Ni-Mo-V type RPV steels have been in use since the 1960s. The Paks VVER-440 reactors were also made out of this type of steel. Instead of developing a completely new tank steel, the manufacturer used decades of experience to develop the previous versions. The amount of Ni was reduced and the amount of impurities (Cu, P, Si) was reduced to the lowest possible amount. With these changes, more favorable mechanical properties and better radiation resistance were achieved. The requirements for mechanical properties are in table 2. (TIMOFEEV & KARZOV, 2006).

Minimum value of				
$R_{p0.2}$ [MPa]*	R_m [MPa]*	A %*	Z %*	DBTT[2]
441	549	15	55	- 25 °C

* *at room temperature*

Table 2. Required mechanical properties of 15H2NMFA steel (TIMOFEEV & KARZOV, 2006)

[2] DBTT = ductile-to-brittle transition temperature

3. EMBRITTLEMENT

The materials of RPV[3]'s (base material, weld material, cladding) show embrittlement during operation. The root of the cause is the neutron radiation and the high temperature. The damage is caused by fast neutrons (>0.5 MeV) and high operating temperatures (~300 °C). The combined effect of fast neutrons and high temperature creates microstructural changes in structural materials (FRAK ET AL., 2015).

The microstructural changes are the following:

- emergence and increase of the density of dislocation loops
- emergence and increase of the density of radiation-induced precipitates
    - Ni, Mn, Si clusters
- increase in the level of grain-boundary segregations of impurities
    - Part of the phosphorus settles on the grain boundary and weakens the binding force between the grains.

As part of the reactor vessel monitoring programs, sets of specimens are irradiated close to the reactor wall and being tested at specified intervals. The purpose of this is to provide real measurement results for the mechanical changes that occur during operation. Since the irradiation channel is closer to the zone than the wall of the container itself, the samples are affected by a higher neutron flux, which leads to accelerated aging.

The tendency to brittle fracture can be described by the shift of the DBTT (Charpy impact test) and the shift of the reference temperature T_0.

- The extent of the transition temperature shift is determined by shifting tangent-hyperbolic curves which were fitted to the Charpy impact test results. The temperature shift corresponding to the impact work value of 41 J is taken into account (OAH 3.18.).
- In the master curve evaluation, the lower envelope corresponding to the 5 % fracture toughness is taken into account. This is accepted in engineering practice, as other safety factors are also used when designing structures (GILLEMOT & HORVÁTH, 2010).

[3] Reactor Pressure Vessel

4. BACKGROUND OF THE REQUIRED MICROSTRUCTURAL AND MECHANICAL INVESTIGATIONS

4.1. Microstructure

The microstructure of a material in this case metal can strongly influence physical properties such as strength, toughness, ductility, hardness. The microstructure can be characterized by the phase composition, texture and presence of defects that make up the material. Structural defects come in many forms. They differ significantly in size and effect. As a first approximation, it is necessary to check whether the material contains continuity defects: pores or cracks. The next range of microstructural defects includes precipitates and inclusions. These defects increase the brittleness of the material (ASM METALS HANDBOOK).

The 15H2NMFA reactor pressure vessel steel is a low alloyed ferritic-pearlitic steel with low carbon content. The texture shows clear ferrite grains and two component pearlite grains (ferrit and cementit laminar structure) (TIMOFEEV & KARZOV, 2006).

The production of reactor pressure vessel for pressurized water nuclear power plants begins with the casting of 100-500 ton ingots. Steel treated in argon-flushing cauldrons under vacuum is poured, thereby minimizing the formation of gas inclusions danger (TIMOFEEV & KARZOV, 2005; SZÉKELY, 2021). As a result, a largely pore-free material can be produced.

Non-metallic inclusions are added to the steel during the manufacturing process. Most of these are carbides (Si-, Fe-, Mo-carbide), oxides (Si-, Mn-oxide) or sulfides (MnS). Golden rule for inclusions: few or none. The amount of inclusions in high-quality steels is very low (VASCONCELLOS, 2018).
Role of the MnS: Manganese is added to all steels in order to prevent the formation of iron sulfide. MnS inclusions are found in most steel (MACIEJEWSKI, 2015).

4.2. Mechanical tests of metallic material

4.2.1. Tensile test

The ASTM E8/E8M standard (Standard Test Methods for Tension Testing of Metallic Materials) was used to perform the tensile tests.

"These test methods cover the tension testing of metallic materials in any form at room temperature, specifically, the methods of determination of yield strength, yield point elongation, tensile strength, elongation, and reduction of area" (ASTM E8/E8M).

4.2.2. Fracture mechanics

From the field of fracture mechanics, I dealt with the calculation of material characteristic parameters (Charpy energy, fracture toughness). As with most engineering structures, the biggest danger for reactor vessels is the brittle fracture. In the case of RPVs, due to fatigue, thermal aging and the destructive effect of neutron radiation, the ductile-brittle transition temperature shifts, so the material becomes continuously more brittle during operation. Test sets are irradiated in the reactors to check the extent of damage.

Charpy test specimens were used for the first time to monitor the shift of the transition temperature and are still used to this day (ASTM E185).

4.2.2.1. Charpy impact test

The ASTM E23 standard (Standard Test Methods for Notched Bar Impact Testing of Metallic Materials) was used to perform the Charpy impact tests.

"These test methods of impact testing relate specifically to the behavior of metal when subjected to a single application of a force resulting in multi-axial stresses associated with a notch, coupled with high rates of loading and in some cases with high or low temperatures. For some materials and temperatures the results of impact tests on notched specimens, when correlated with service experience, have been found to predict the likelihood of brittle fracture accurately." ASTM E23.

In summary, with this technique it is easy to determine how much invested work is required to break the material in case of dynamic stress. Figure 3. shows the principle operation of the equipment. A hammer on a pendulum strikes the test specimen and the amount of absorbed energy can be determined from the difference in the potential energies.

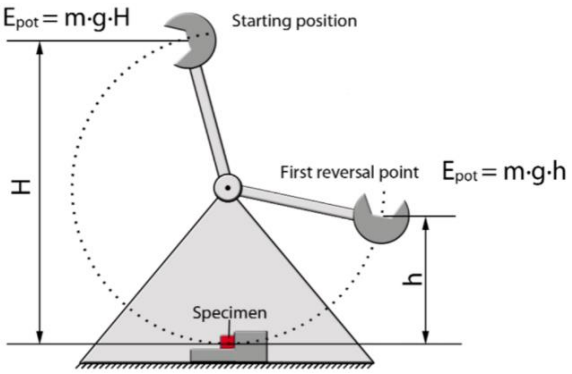

Figure 3. Drawing of the Charpy impact test (*911metallurgist.com*)

The specimen is placed on a standard size anvil (Figure 4.). Between the anvils the distance is 40 mm. This guarantees that the same stress state is always created and that the different measurement results can be compared.

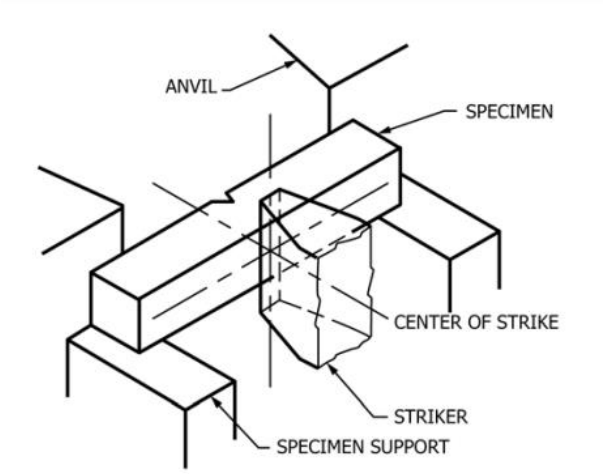

Figure 4. Charpy anvil (*ASTM E23 Standard*)

The notch is of great importance for the test results (KURISHITA ET AL., 1993). During the test, I used a V-type specimen with a 2 mm deep 0.25 mm radius notch (Figure 5.). The size of the sample can also affect results (MILLS, 1976). I used 10 x 5 x 55 mm size specimens.

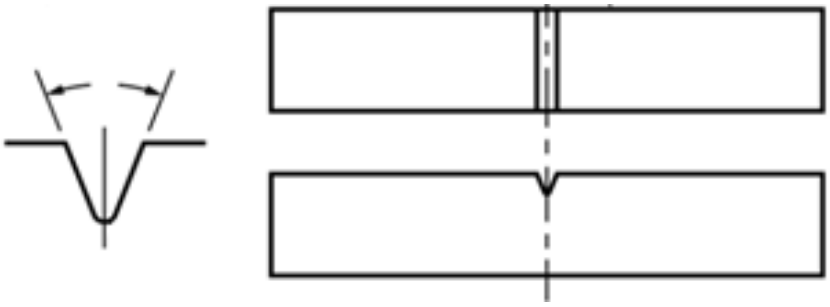

Figure 5. Charpy specimen (*ASTM E23 Standard*)

Qualitative and quantitative results can be obtained from charpy impact tests:

A qualitative result is the determination of the plasticity of the material (MATHURT ET AL., 1994). If the fracture surface is smooth and no traces of plastic deformation are visible, then we are talking about a brittle fracture. If jagged edges and shear marks are visible on the fracture surface, then this fracture is ductile (MEYERS & CHAWLA, 1998).

A quantitative result, if we determine how much energy was needed to break the material. If we perform the test at different temperatures, we can determine the energy required to break a material as a function of temperature. The ductile-brittle transition is not a sharp boundary (Figure 6). More like a range. Many countries have their own DBTT (ductile to brittle transition temperature) standards. The value corresponding to 41 J is accepted, but the value corresponding to 43 J and 47 J is also used (GILLEMOT & HORVÁTH, 2010).

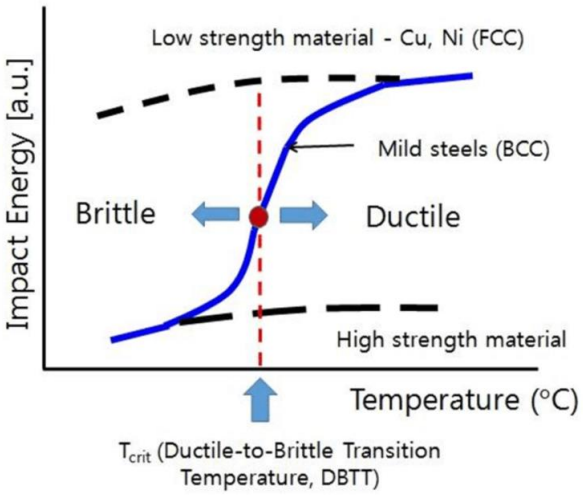

Figure 6. Temperature versus impact energy curve (*yenaengineering.nl*)

The transitional temperature value calculated from the evaluation of the Charpy specimens and its subsequent shift can only be considered an approximation. As shown above, the Charpy-V impact test is performed on a specimen with a rounded 0.25 mm radius notch. However the fracture work we measure, consists of several components: the deformation work necessary from the rounded notch to the initiation of the crack, the work of crack initiation and the work of crack propagation through the entire thickness of the specimen. The determination of the transition temperature is based on some empirical criteria (absorbed energy: 41, 43, 47 J; lateral expansion or fracture evaluation), which was developed in the railway industry, without a physical background (GILLEMOT & HORVÁTH, 2010).

4.2.2.2. Introduction to master curve theory

As the temperature decreases, the fracture toughness of structural steels decreases dramatically. Their fracture shows a gradual transition from fully ductile to brittle fracture. Determining the transition temperature required the development of elastic-plastic fracture mechanics. It was a huge problem that large test specimens were needed to carry out the tests. Routine examination of large specimens is not easy, and their irradiation in a reactor is not possible. In the 1970s, an ad hoc PVRC [4]group began collecting all available valid fracture toughness, Charpy impact work, and drop-weight data. The master curve is actually an exponential curve that describes the change in fracture toughness as a function of temperature (McCabe et al., 2005).

A real material parameter, the value of fracture toughness, is used in the evaluation. In material testing, fracture toughness is a material characteristic that shows the material's resistance to fracture when it contains a crack (production or fatigue). Fracture toughness is the work value at which the crack starts under static load.

For the calculations, the critical value of fracture toughness is K_{IC} = 100 $MPam^{1/2}$, which is measured on small specimens and converted to 1 CT data using the weakest link and semi-empirical estimation. The master curve is a semi-empirical approximation of the fracture toughness trend curve. The temperature corresponding to a value of 100 Mpam1/2 is called the reference temperature (T_0) (GILLEMOT & HORVÁTH, 2010).

[4] Pressure Vessel Research Committee

4.2.2.3. Determination of T_0 reference temperature

The ASTM E1921 standard (Standard Test Method for Determination of Reference Temperature, T_0, for Ferritic Steels in the Transition Range) was used to determine the T_0 reference temperature.

Master curve evaluation

The master curve evaluation can be done by measuring at one temperature. It only requires simple calculations, but it is very difficult to guess at first which measurement temperature gives the fracture toughness of 100 $MPam^{1/2}$, so the first few measurements will probably be invalid. The analysis at multiple temperatures (Eq. 2.) requires a more complex mathematical evaluation, but probably all measurement results can be evaluated. There are only two criteria to be followed during the evaluation. The difference between the test temperature and the value of T_0 can be max. ±50 °C. In addition, the measurement deviation (σ) must be taken into account (Eq.1.).

$$\sigma = \sqrt{\frac{\beta^2}{r} + \sigma_{exp}^2}\,, \tag{1}$$

where:

β = sample size uncertainty factor,

r = total number of uncensored data,

σ_{exp} = contribution of experimental uncertainties (in practice σ_{exp} = 4 °C) .

Equation for multi-temperature analysis:

$$\sum_{i=1}^{N} \delta_i \frac{exp\left[0.019\left(T_i - T_{0Q}\right)\right]}{11 + 77exp\left[0.019\left(T_i - T_{0Q}\right)\right]} - \sum_{i=1}^{N} \frac{\left(K_{Jc(i)} - 20\right)^4 exp\left[0.019\left(T_i - T_{0Q}\right)\right]}{\left\{11 + 77exp\left[0.019\left(T_i - T_{0Q}\right)\right]\right\}^5} = 0 \tag{2}$$

where:

N = number of specimens tested,

T_i = test temperature corresponding to KJc(i),

$K_{Jc(i)}$ = either an uncensored K_{Jc} datum or a datum replaced with a censoring value

K_{Jc} = critical fracture toughness value calculated from J integral[5]

T_{0Q} = estimated T_0

δ_i = 1.0 if the datum is uncensored or zero if the datum is a censored value,

11 = integer equivalent of $10/(\ln 2)^{1/4}$ MPa√m,

77 = integer equivalent of $70/(\ln 2)^{1/4}$ MPa√m

The K_{Jc} value is required to perform the analysis. We can get this by solving the following equation (Eq. 3):

$$K_{Jc} = \sqrt{J_c \frac{E}{1-\nu^2}} \ , \tag{3}$$

Where:

ν = Poisson's ratio

J_c = critical value of J integral

E = elastic modulus

Determining the value of K_{Jc} is a multi-step process, which consists of the following steps:

- The yield strength (σ_{ys}) (Eq. 4.) and modulus of elasticity (E) (Eq.5.) change with temperature. The data measured at RT must be converted to the temperature of the fracture measurements using the equations below:

$$\sigma_{ys} = \sigma_{ysRT} + \frac{10^5}{(491 + 1.8T)} - 189 \, , \tag{4}$$

where:

T = test temperature (°C)

σ_{ysRT} = the material yield strength at room temperature (MPa)

[5] "The **J-integral** represents a way to calculate the strain energy release rate, or work (energy) per unit fracture surface area, in a material." (Van vliet)

$$E = 204 - \frac{T}{16}\,, \tag{5}$$

where:

T = test temperature

- The next step is to determine J_c (the critical value of the J integral) (Eq.6.). The elastic (Eq.7.) and plastic (Eq.10.) deformation around the crack must be taken into account and the geometry of the sample (Eq. 8-9.).

$$J_c = J_e + J_p\,, \tag{6}$$

where:

J_c = critical value of J integral

$$J_e = \frac{(1-\nu^2)K_e^2}{E}\,, \tag{7}$$

$$K_e = \left\{PS/\left[(BB_N)^{1/2}W^{3/2}\right]\right\} f(a_0/W)\,, \tag{8}$$

$$f(a_0/W) = \frac{3(a_0/W)^{1/2}}{2[1+2(a_0/W)]}\left[\frac{1.99-(a_0/W)(1-a_0/W)\left[2.15-3.93\left(\frac{a_0}{W}\right)+2.7(a_0/W)^2\right]}{(1-a_0/W)^{3/2}}\right], \tag{9}$$

$$J_p = \frac{\eta A_p}{B_N b_0}\,, \tag{10}$$

where:

$A_0 = A - 1/2C_0P^2$,

$A = A_e + A_p$,

C_0 = reciprocal of the initial elastic slope,

b_0 = initial remaining ligament

a_0 = initial crack length

- If the measured fracture toughness value is greater than the calculated value (Eq.11.), i.e. no brittle fracture or quasi-brittle fracture occurred, then the calculated value must be used. All measurement data must be censored.

$$K_{Jclimit} = \sqrt{\frac{Eb_0\sigma_{YS}}{30(1-\nu^2)}} \tag{11}$$

- The censored and uncensored K_{Jc} values must be converted to 1 CT specimen using the formula below (Eq.12.):

$$K_{Jc(x)} = 20 + \left[K_{Jc(0)} - 20\right]\left(\frac{B_0}{B_x}\right)^{1/4}, \tag{12}$$

where:

$K_{Jc(x)}$ = K_{Jc} for a specimen size B_x,

$K_{Jc(0)}$ = K_{Jc} for a specimen size B_0,

B_0 = gross thickness of test specimens,

B_x = gross thickness of prediction (25.4 mm)

5. RESULTS

5.1. Microstructure of 15H2NMFA

The microstructure tests were performed based on the ASTM E3 (Standard Guide for Preparation of Metallographic Specimens) E407 (Standard Practice for Microetching Metals and Alloys) standards.

I made a cross-section cut from the sample. After polishing, I inspected the surface for pores. The sample did not contain pores. I then examined the sample with polarized light. With the help of this, the non-metallic inclusions became visible (Figure 7.). I identified the chemical composition of the inclusions with electron microscopic EDS measurements: MnS (Figure 8.). The grain size of the MnS inclusions is between few µm – 30 µm.

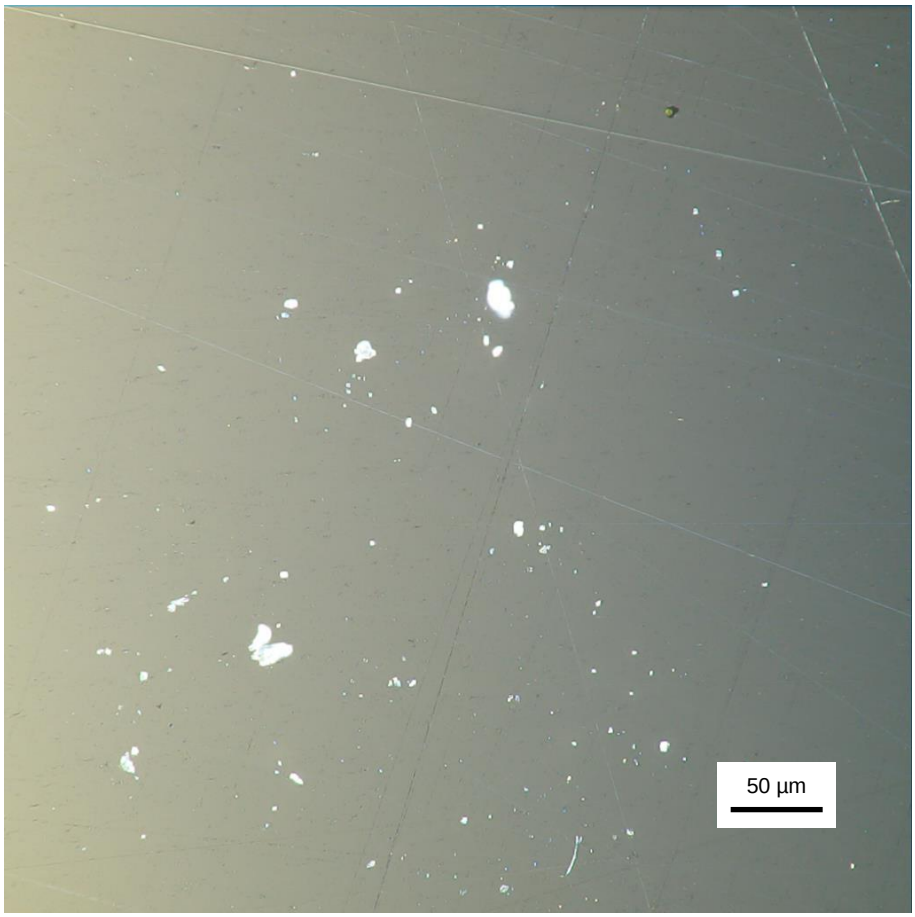

Figure 7. Cross-section of 15H2NMFA steel with polarized light

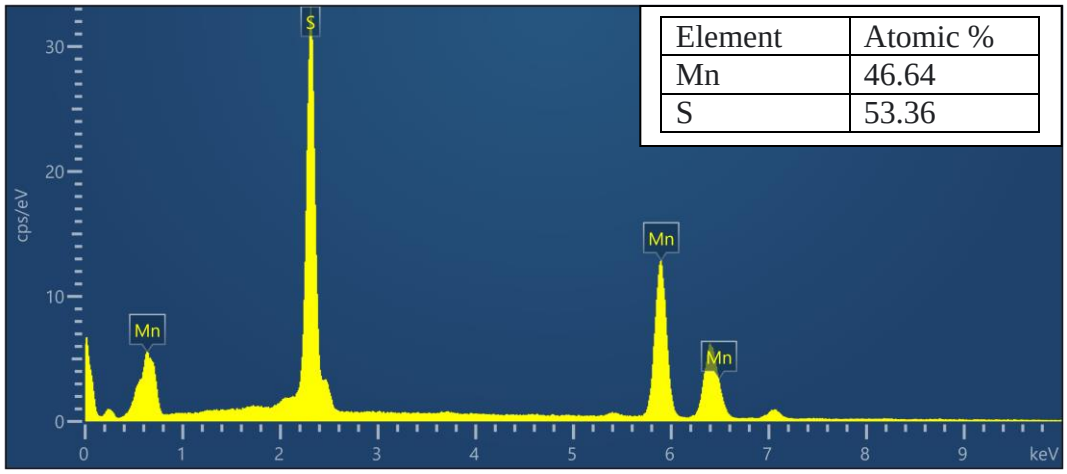

Element	Atomic %
Mn	46.64
S	53.36

Figure 8. EDS spectra of the inclusions

In the second step, I etched the sample so that the textural elements became visible (Figure 9.). I used 2% nital (methanol + nitric acid) for this.

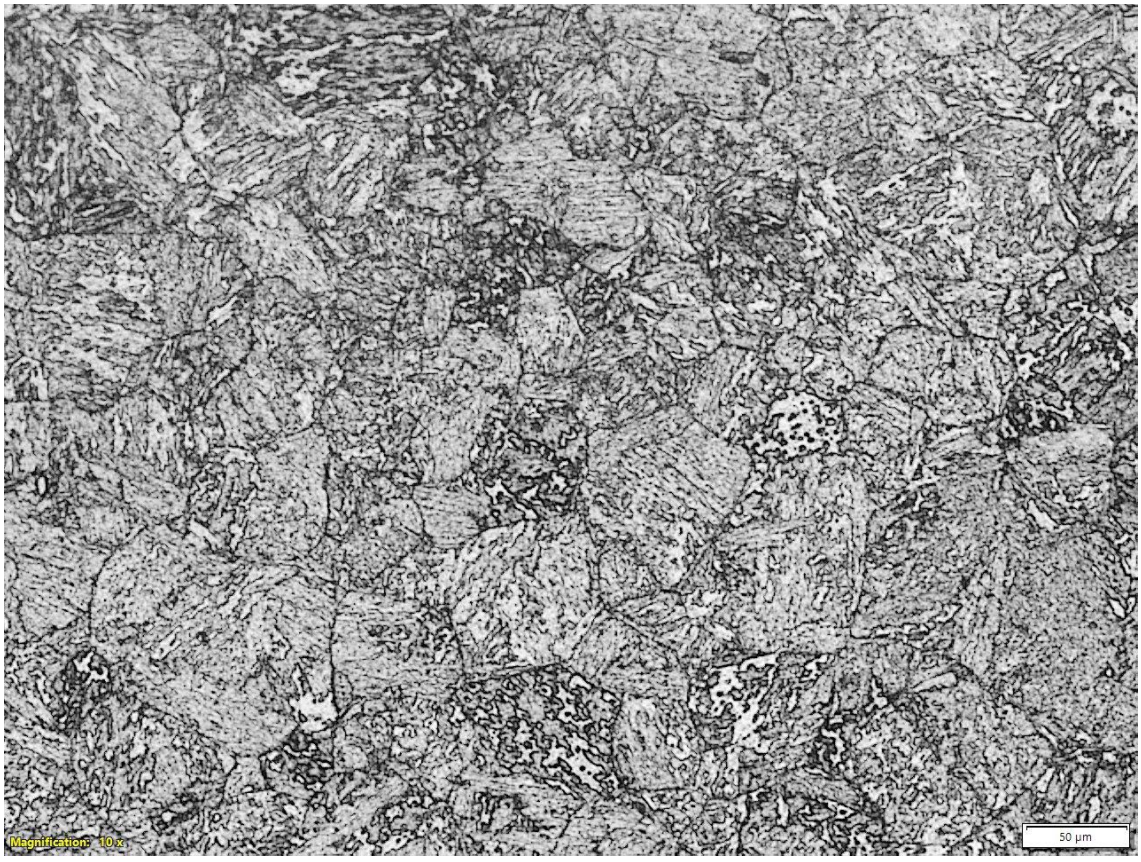

Figure 9. Etched cross-section of 15H2NMFA steel

A typical ferritic-pearlitic microstructure, the grain size does not exceed 100 µm.

5.2. Mechanical tests of 15H2NMFA steel

5.2.1. Tensile test

In order to decide whether the material shows inhomogeneity or harmful hardening that occurred during the production of the samples, I used Vickers hardness measurement on the samples – 1 kg load on five points (Table 3.). The hardness of the specimens is within the normal scatter of the hardness testing.

Hardness testing (HV1)						
Code	1	2	3	4	5	Average
S2	273.0	268.8	285.4	255.9	283.8	273.4
S3	279.6	258.4	260.5	258.2	266.0	264.6
S4	257.8	278.1	269.3	270.2	274.1	269.9
					Average	269.3

Table 3. Hardness testing results of tensile specimens

The tensile testing made on room temperature, on flat specimens (L direction) with 5 x 5 mm cross section. The geometry parameters are in the table 4. The testing machine was an Instron 8801 servo-hydraulic testing system. The testing speed is 0.5 mm/minute. The results are summarized in table 5. and figure 10. The error of the optical measuring system and the force-measuring cell is also 0.1%. The error in the result is negligible.

Sample parameters					
Code	a [mm]	b [mm]	L [mm]	L_0 [mm]	A_0 [mm^2]
S2	4.98	4.99	60	24	24.85
S3	5.00	5.00	60	24	25.00
S4	5.00	4.99	60	24	24.95

Table 4. Geometry parameters of the tensile specimens

Results								
Code	au [mm]	bu [mm]	Au [mm^2]	Lu [mm]	A [%]	Z [%]	$R_{p0.2}$ [MPa]	R_m [MPa]
S2	2.85	2.88	8.21	30.26	26	67	593	692
S3	2.55	2.83	7.22	30.67	28	71	589	691
S4	2.57	2.66	6.84	30.25	26	73	592	692

Table 5. Results of the tensile test

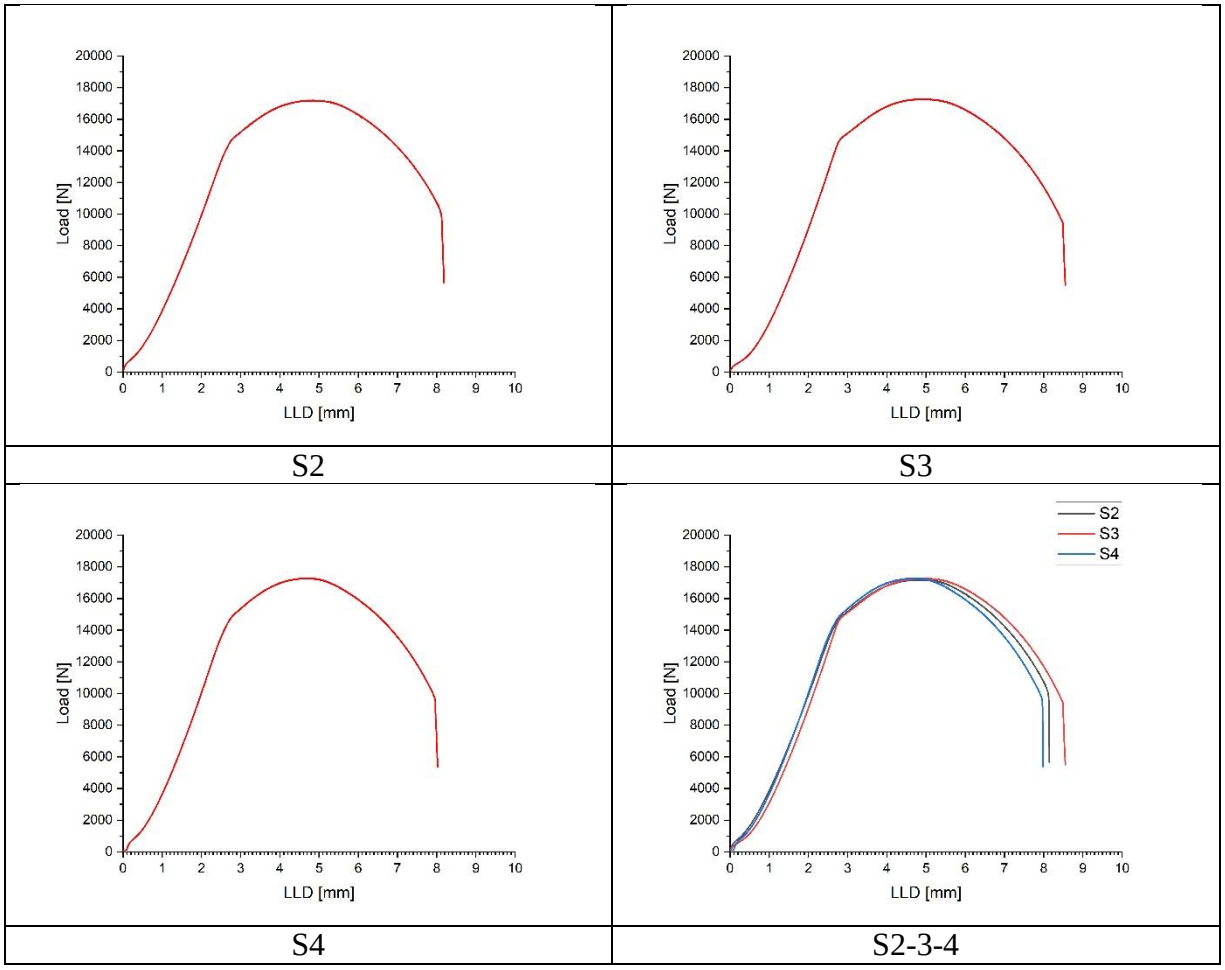

Figure 10. Tensile curves of the test specimens

The curves move together. The values of slope, yield strength and tensile strength show negligible deviations from the average.

Young's modulus

The Young's modulus (E) quantifies the relationship between the tensile stress (σ) and axial strain (ε) in the linear-elastic region (Eq 13.) (JASTRZEBSKI, 1959).

$$E = \frac{\sigma}{\varepsilon} \tag{13}$$

The modulus of elasticity can be determined from the tensile curve. Young's modulus is obtained by calculating the slope of the curve in the linear-elastic range. The calculated elastic modulus is 208 GPa.

Poisson's ratio

Poisson's ratio (v) is a number used in the mechanics of solid materials. In the case of a unidirectional stress state, the relationship between transverse strain and longitudinal strain. By substituting the results of the 5-th table into the equation below (Eq.14.), we get the Poisson's ratio of the material (JASTRZEBSKI, 1959).

$$\frac{\Delta d}{d} = -v\frac{\Delta L}{L}, \tag{14}$$

Where d is the original thickness, L is the length, Δd is the changed thickness and ΔL is the changed length. The calculated Poisson's ratio (v) is 0.33.

Optical investigation

Real structural materials are not always homogeneous, small and large inclusions occur in the material. Uniform stretching means uniaxial stress distribution. The inclusions reduce the load-bearing capacity of the cross-section and create a local multi-axial stress distribution. After the measurement, I performed optical (Figure 11-13.) and electron microscopic (Figure 14-16.) examination of the fracture surfaces.

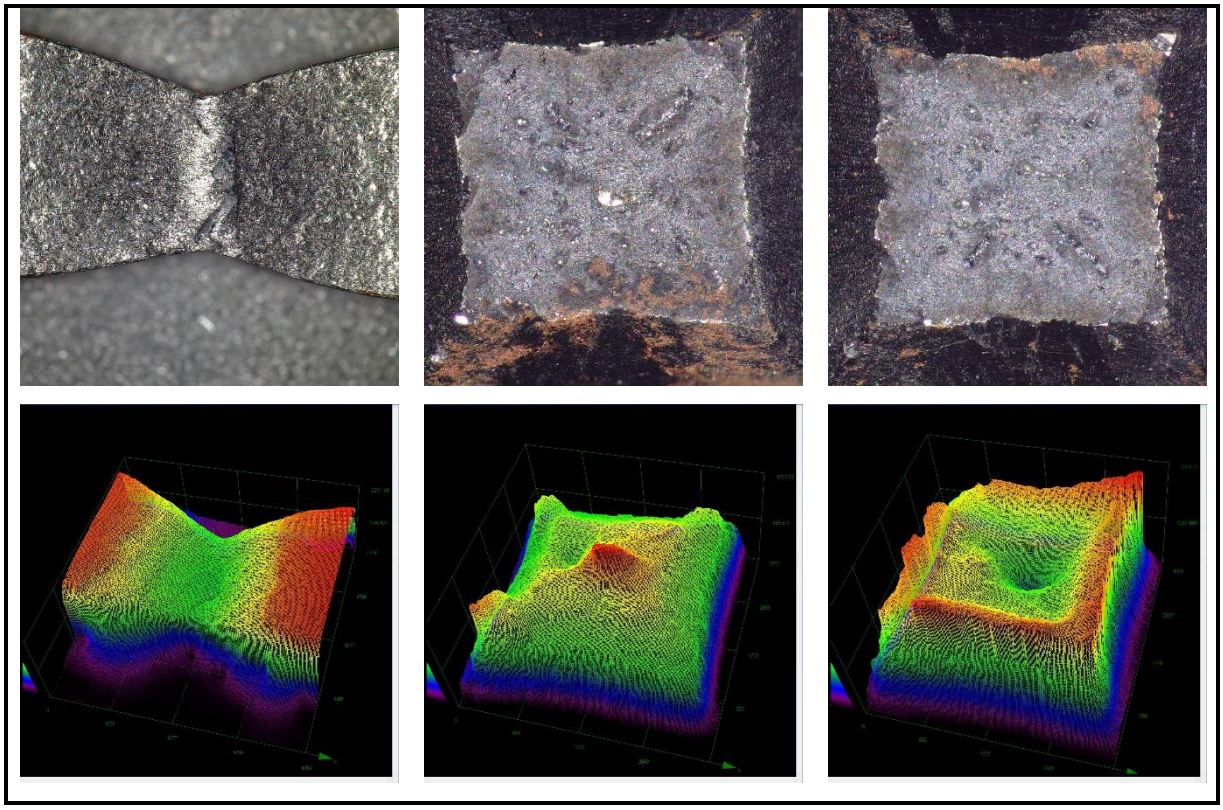

Figure 11. S2 test specimen fracture surface optical and height-contrast images

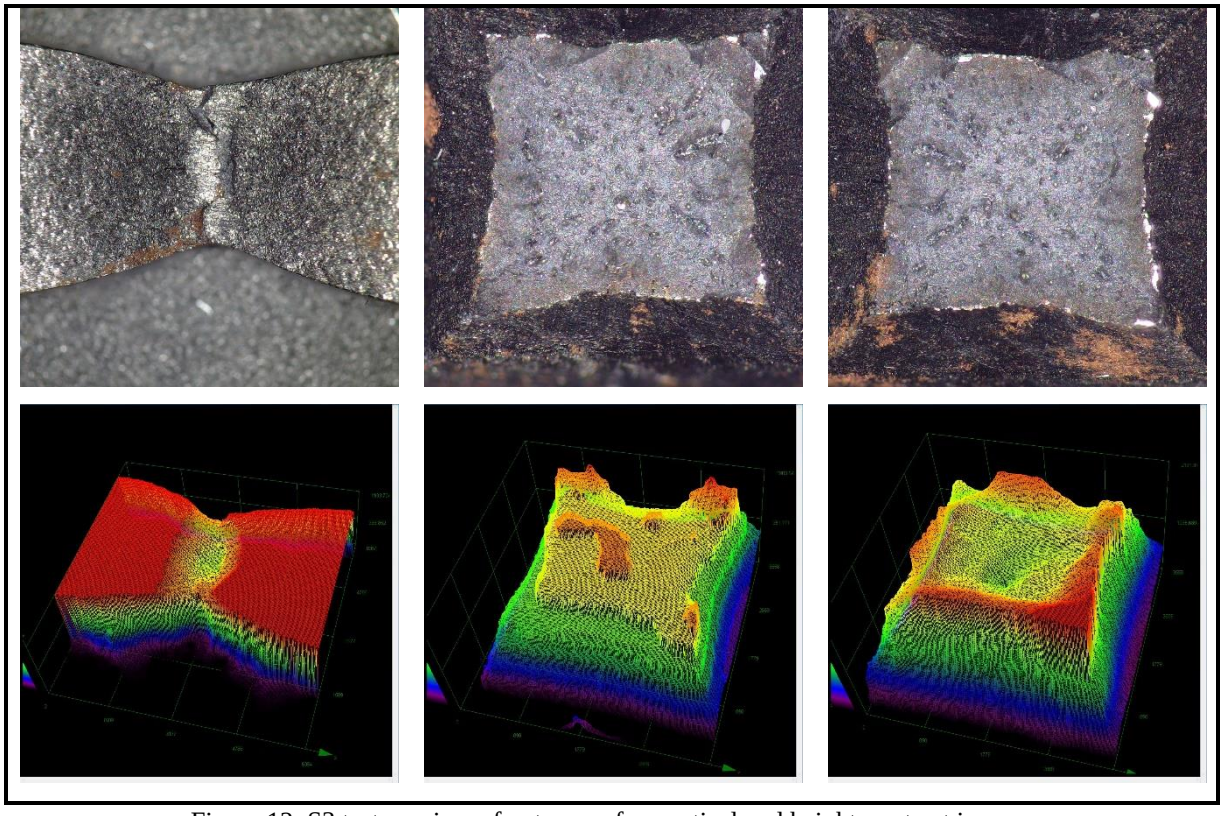

Figure 12. S3 test specimen fracture surface optical and height-contrast images

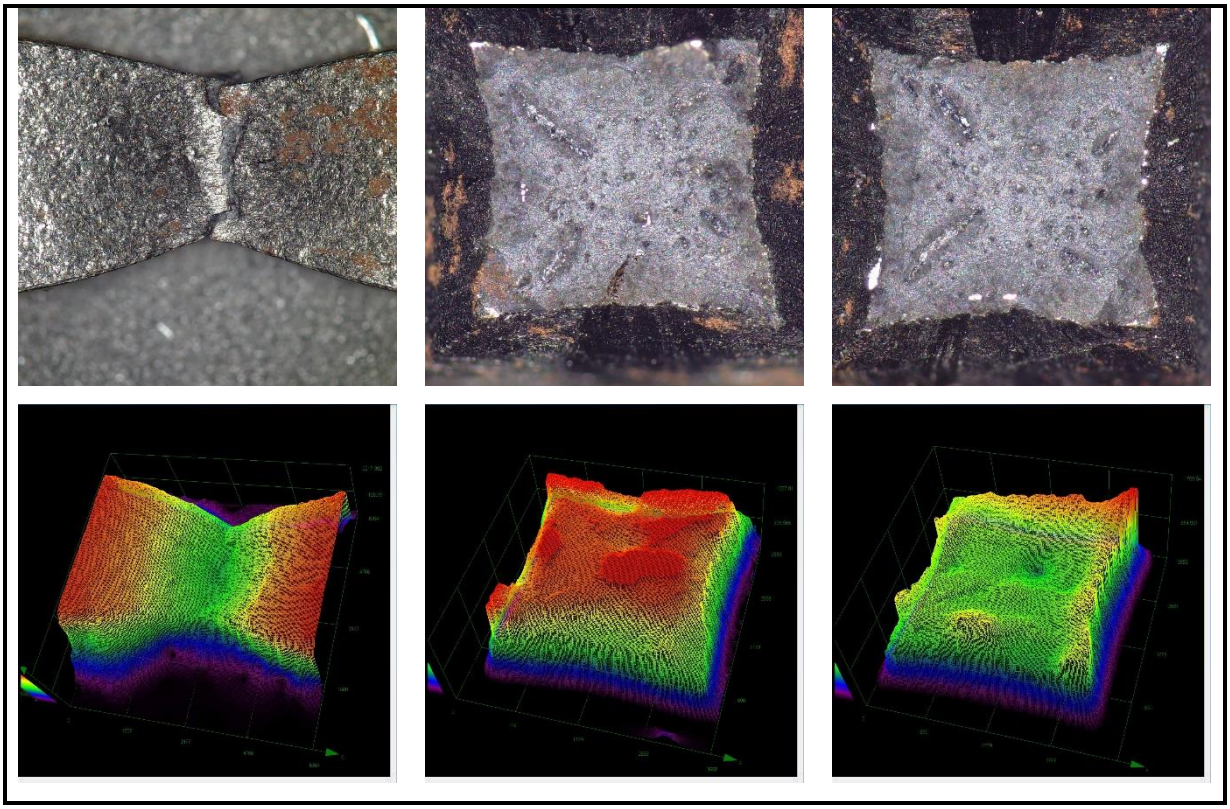

Figure 13. S4 test specimen fracture surface optical and height-contrast images

I performed the fractographic analyzes on the fracture surfaces with an Olympus DSX1000 type optical microscope. No inclusions or gas cavities are visible on the surfaces. For a better analysis of the contracted section, I took 3D height-contrast images. It is clearly visible that the cross-section is significantly reduced (Z>10%) and the specimen has undergone strong plastic deformation.

Sample: S2	
Sample preparation: *Carbon tape*	
Environment: *High vacuum*	
Acc. volt.: *5-15 keV*	WD*:* 10 mm

Observations:

Low magnification: Strong contraction

High magnification: No inclusions, highly ductile surface

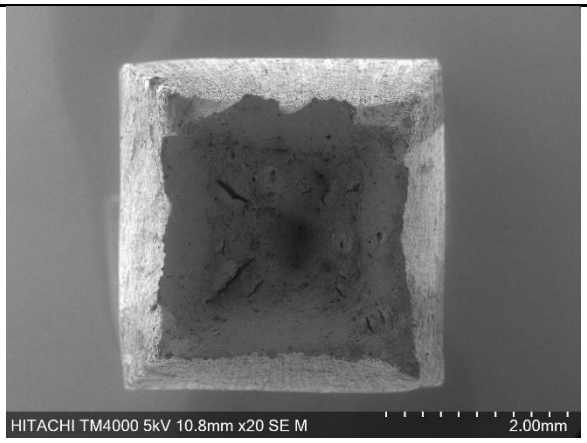

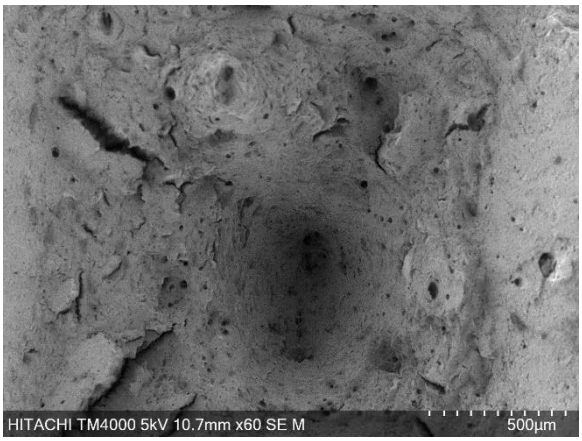

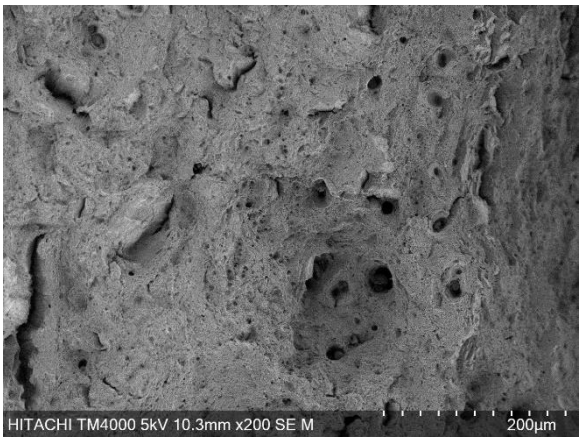

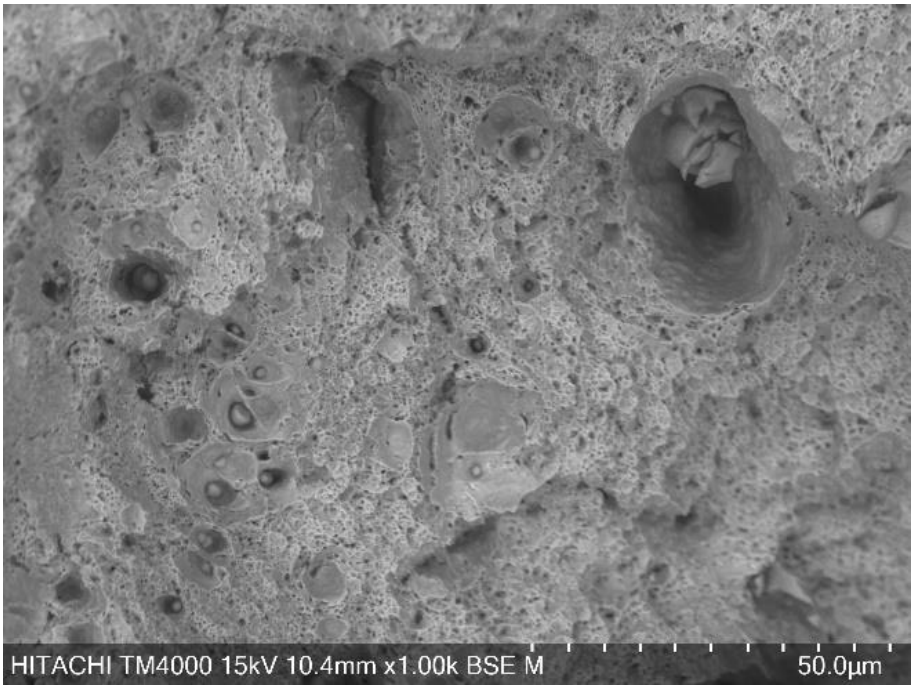

Figure 14. S2 test specimen fracture surface electron microscopic images

Sample: S3

Sample preparation:	*Carbon tape*
Environment:	*High vacuum*
Acc. volt.: *5-15 keV*	WD*: 10 mm*

Observations*:*

Low magnification: Strong contraction

High magnification: No inclusions, highly ductile surface

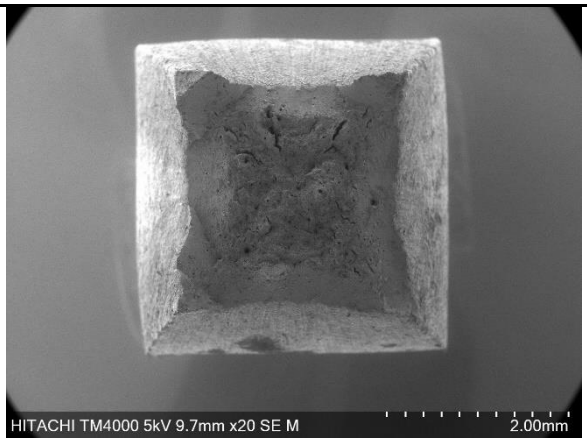

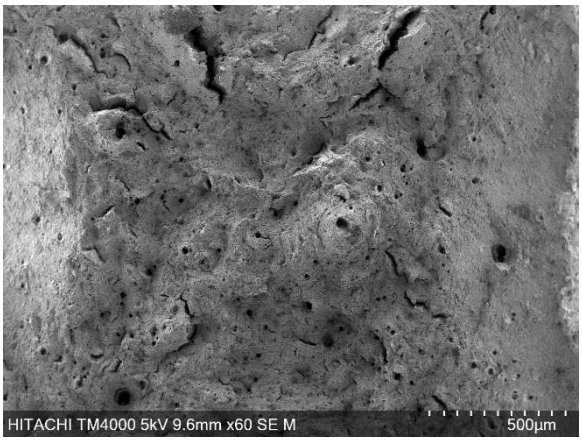

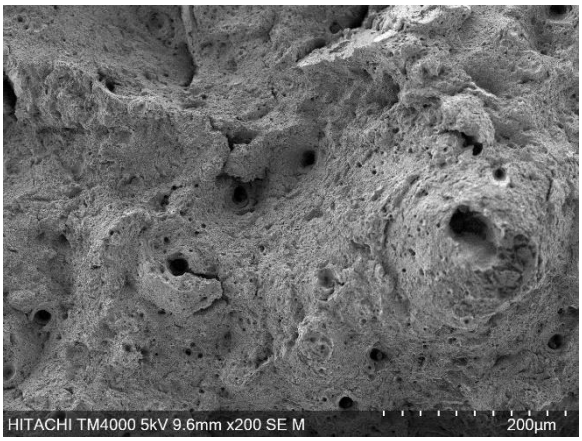

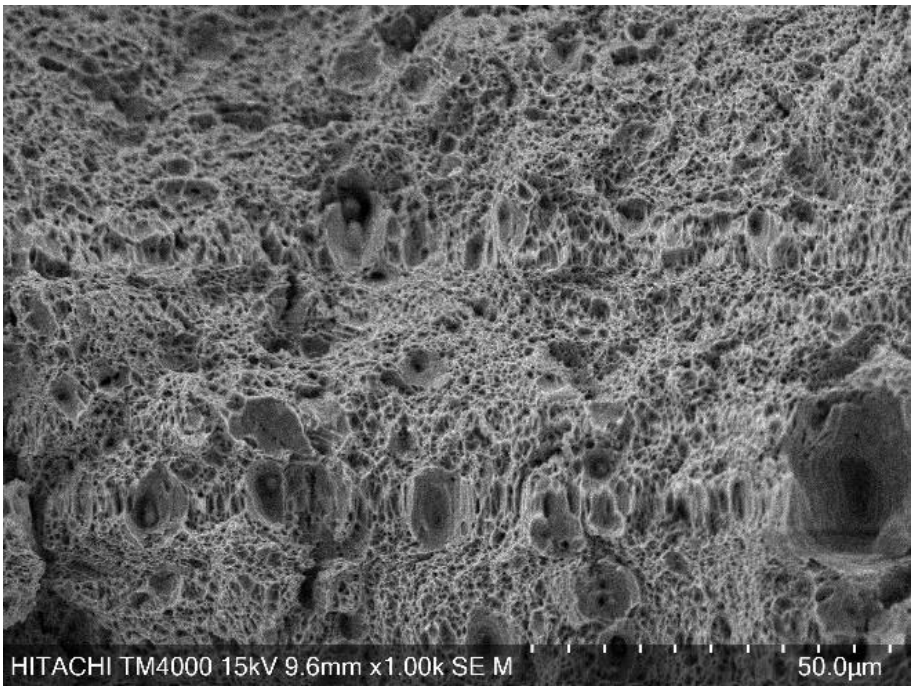

Figure 15. S3 test specimen fracture surface electron microscopic images

Sample: S4		
Sample preparation:	*Carbon tape*	
Environment:	*High vacuum*	
Acc. volt.: *5-15 keV*	WD*: 10 mm*	

Observations:

Low magnification: Strong contraction

High magnification: No inclusions, highly ductile surface

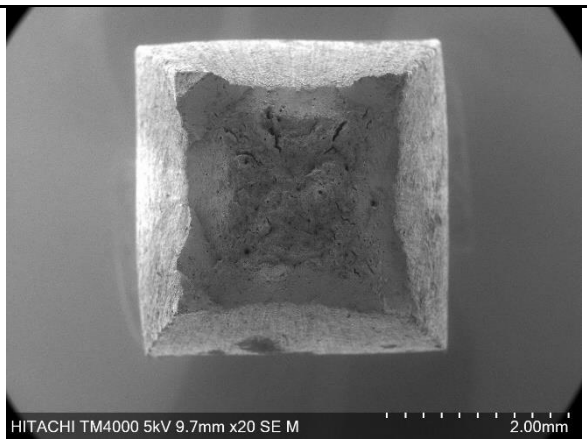

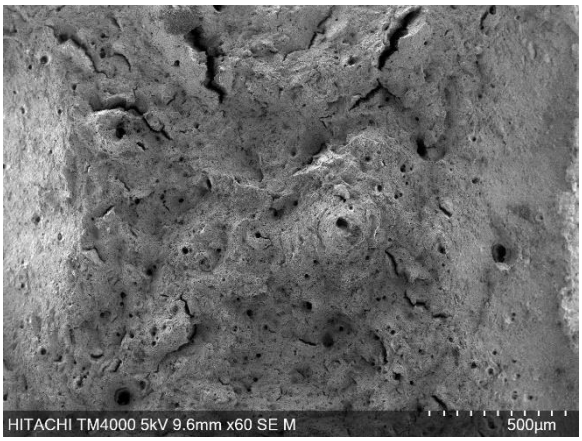

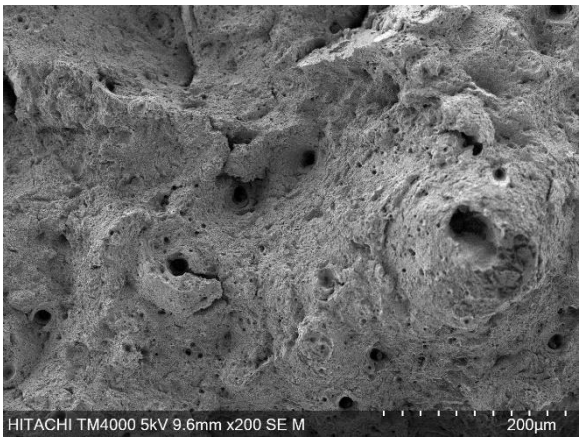

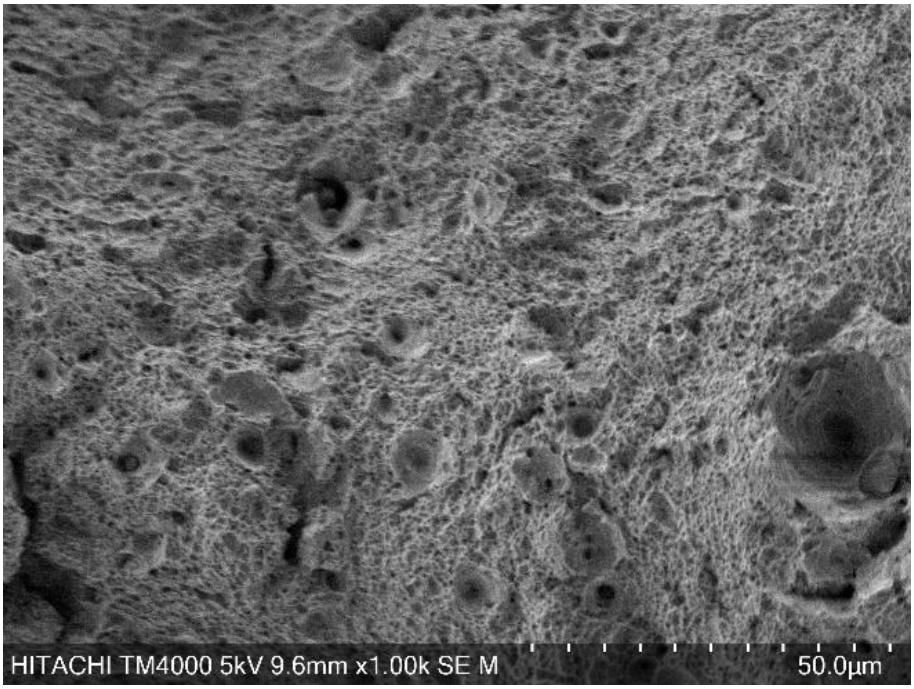

Figure 16. S4 test specimen fracture surface electron microscopic images

5.2.2. Fracture mechanics

5.2.2.1. Charpy impact test

Technical background of Charpy impact test:

Charpy impact testing made using a 300 J capacity impact tester. The specimens cooled to the testing temperature in liquid n-pentane. The temperature of the cooling media measured by two independent K-type thermocouple (accuracy ±2°C). One of the thermocouples brazed into a Charpy size steel block. This block inserted into the cooling media together with the specimens. The cooling media temperature adjusted by using a heat exchanger. Vapor of liquid nitrogen used for cooling in the heat exchanger. The temperature controlled by the flow control of the nitrogen vapor. The specimens located into the fixture of the impact machine by a cooled forceps. The testing performed within 3 seconds after the specimen taken out from the liquid.

The specimens are half thick Charpy specimens. Kim Wallin (KIM WALLIN, 2016) methodology is used to convert the data for standard Charpy size (10 x 10 x 55 mm). Charpy impact experimental data have to be approximated by hyperbolic tangent function (x) that designates the transition temperature (Eq.15.). This curve shows the relationship between the impact absorption energy and test temperature (ORYNYAK ET AL., 2013). A summary of the Charpy test data can be seen in table 6.

$$E(T) = A + B \cdot th\left(\frac{T - T_0}{C}\right), \tag{15}$$

where: A, B, C and T_0 – empirical constants determined using least squares method; T – temperature; E(T) – function determining the relation between Charpy impact energy and temperature (Figure 17.).

Code	L [mm]	w [mm]	B [mm]	a [mm]	R [mm]	T [°C]	Energy [J]	Lateral expansion [mm]
R1	55.02	9.98	5.00	2.00	0.25	22	73	1.17
R2	55.00	9.99	5.00	2.02	0.25	22	54	1.49
R3	55.02	9.99	4.99	2.00	0.25	22	54	1.45
R4	55.01	9.99	4.99	2.02	0.25	-20	40	1.22
R5	54.98	9.99	5.00	2.02	0.25	-20	31	0.88
R6	54.99	9.99	5.00	2.00	0.25	-20	32	0.78
R7	55.04	9.98	4.99	2.00	0.25	-30	32	0.88
R8	55.00	10.00	5.00	2.00	0.25	-30	32	0.84
R9	55.01	10.00	4.99	2.00	0.25	-30	32	0.91
R10	55.00	9.99	4.99	2.00	0.25	-40	29	0.7
R11*	55.01	9.99	5.00	2.01	0.25	-40	6	0.05
R12	54.99	9.99	5.00	2.00	0.25	-40	16	0.48
R13	54.99	9.98	4.99	2.02	0.25	-52	30	0.76
R14	55.00	9.99	4.99	2.00	0.25	-52	20	0.45
R15	54.98	9.99	5.00	2.00	0.25	-52	30	0.71
R16	54.99	9.99	4.99	2.01	0.25	-72	28	0.73
R17*	54.99	9.98	4.99	2.03	0.25	-72		0.83
R18	55.00	9.99	5.00	2.00	0.25	-62	24	0.69
R19*	55.01	9.99	4.99	2.00	0.25	-62	8	0.26
R20	54.98	9.99	5.00	2.00	0.25	-62	34	0.81

Table 6. Charpy test data

Fractography of specimen R11 and R19 shown defects at the fracture surface. At the testing of R17 the energy value lost. These specimens are not used at the evaluation.

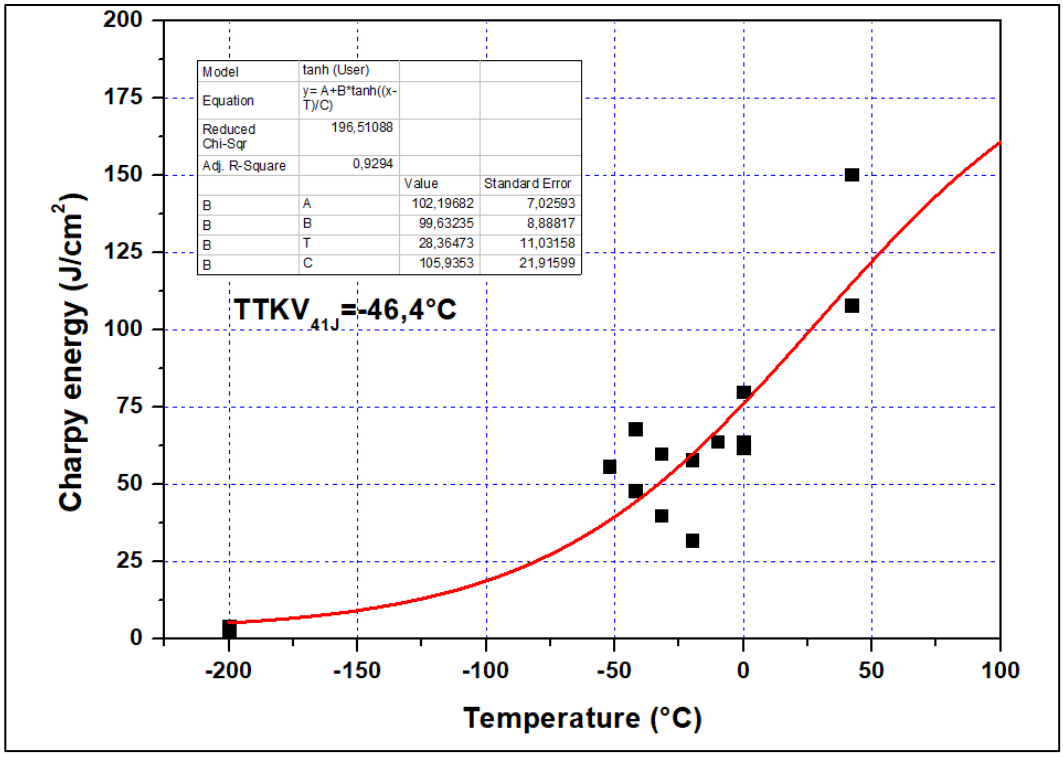

Figure 17. The tangent hyperbolic curve fitted to the plotted measurement results

The calculated $TTKV_{41J}$= - 46.4 ± 2 °C.

5.2.2.2. Master curve – T_0 determination

Figure 18. shows the principle operation of the test. To determine the fracture toughness, I used three point bend fracture mechanics test specimens. Their geometry is 10 x 5 x 55 mm (Figure 19.). In the case of a TPB specimen, the load acts in the plane of the crack. The distance between the support rollers is 40 mm (S/w = 4). The specimens are cooled inside a large copper block. Vertical holes were drilled into the copper block, through which liquid nitrogen flows. The good heat transfer of copper and the internal design of the cooling device allow the test pieces to cool down quickly and keep the temperature surface stable during the measurement.

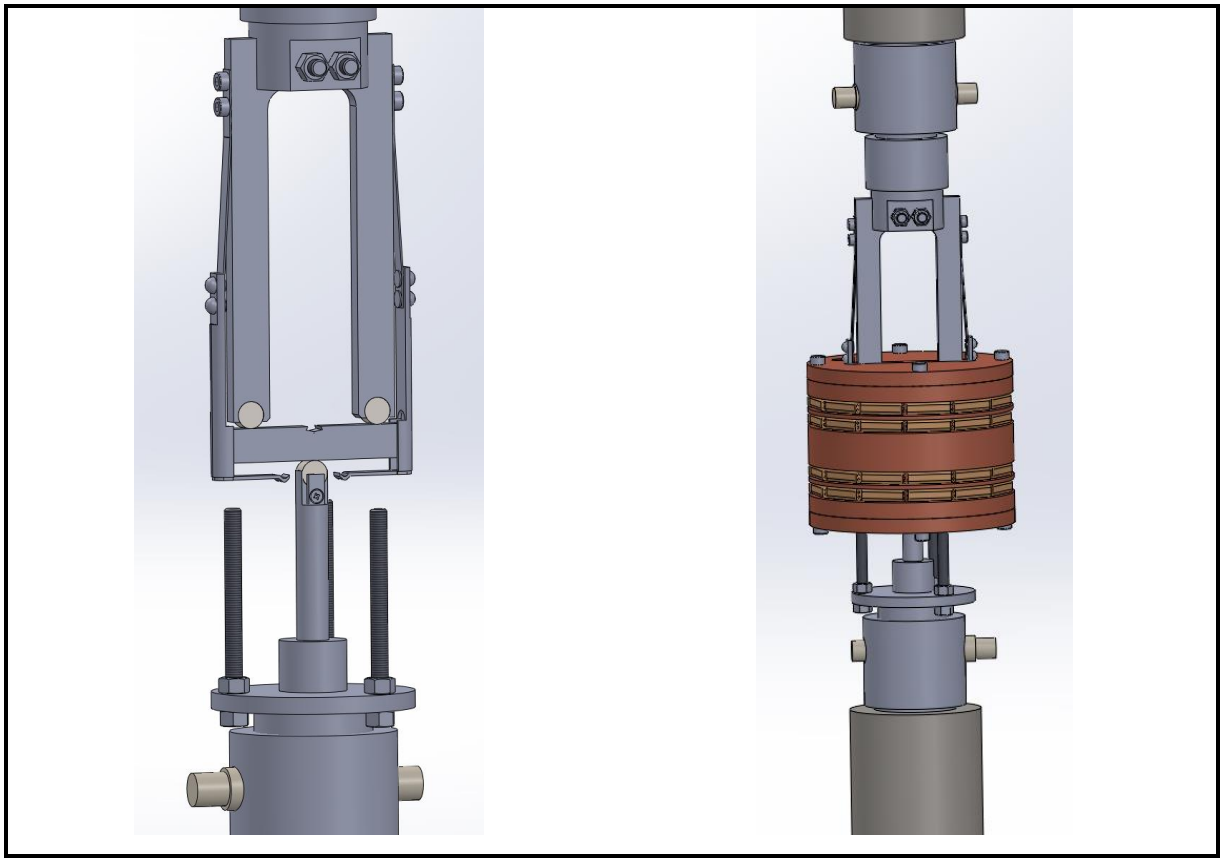

Figure 18. 3D model of the press tool and cooling-heating equipment designed for fracture mechanics tests

In the first step, I checked the samples dimensions. Everything was within the size limits specified in the standard (Table 7.)

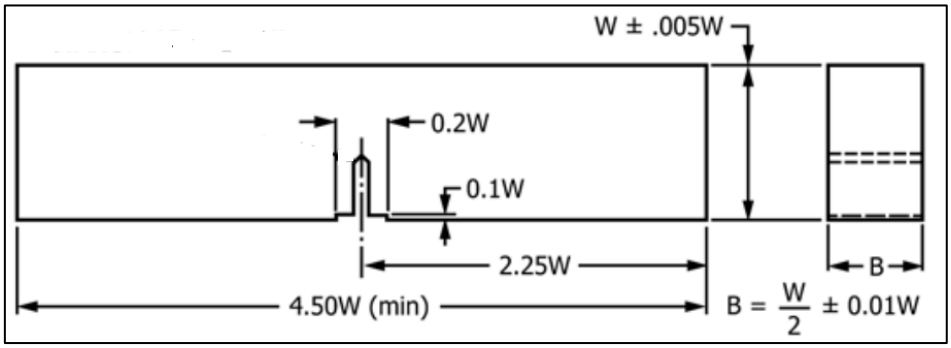

Figure 19. Drawing of the TPB specimen (*ASTM E1921*)

	W [mm]	B [mm]
R21	10.00	5.00
R22	9.99	5.00
R23	9.98	5.00
R24	9.99	5.00
R26	9.98	4.98
R27	9.98	4.99
R28	9.98	5.00
R29	9.99	5.00
R30	10.00	4.99
R31	10.00	4.99
R32	10.00	5.00
R33	10.00	4.99
R34	9.99	5.01
R39	9.99	5.00

Table 7. Geometry parameters of the TPB specimens

In order to decide whether the material shows inhomogeneity or harmful hardening that occurred during the production of the samples, I used Vickers hardness measurement on the samples – 1 kg load on five points (Table 8.). The hardness of the specimens shows slightly high scatter, but it is within tolerance.

Hardness testing (HV1)						
Code	1	2	3	4	5	Average
R21	221.6	233.7	230.8	226.0	227.1	227.8
R22	245.9	257.5	255.9	224.4	237.5	244.2
R23	261.5	264.5	258.4	255.6	255.0	259.0
R24	236.6	229.2	225.1	247.7	235.3	234.8
R26	247.5	245.7	241.0	241.6	242.1	243.6
R27	244.7	246.9	247.8	246.3	241.3	245.4
R28	236.8	241.9	242.8	243.1	245.4	242.0
R29	247.6	248.0	243.3	243.6	247.0	245.9
R30	239.5	241.0	239.3	243.3	242.4	241.1
R31	285.3	276.5	294.0	301.1	271.1	285.6
R32	269.4	276.7	278.6	269.6	277.0	274.3
R33	295.9	283.9	271.3	272.5	272.6	279.2
R34	250.8	243.1	244.4	249.3	250.6	247.6
R39	248.4	263.8	224.7	245.4	238.2	244.1
R40	255.8	260.2	240.0	249.2	256.7	252.4
					Average	**251.1**

Table 8. Hardness testin results of the TPB specimens

The notches on the test specimens were made with thin wire EDM. No matter how thin the wire is, the mechanical incision will have a radius. In order to create a sharp crack on the specimen, pre-fatigue is necessary. The fatigue was performed at room temperature and in the range between K = 25-15 $Mpam^{1/2}$, while reducing the force in several steps. R = 0.1. Cycle number: 40,000 – 100,000. Gradual reduction of the fatigue force is useful, on the one hand, because the crack does not run too far, and on the other hand, the smallest possible plastic zone is created around the crack tip by applying an ever-smaller force.

The R40 sample was used to test the measuring system. It was loaded at room temperature and was not taken into account in the evaluation. The fracture mechanics tests were performed on an Instron 8801 servo-hydraulic universal test machine. In the first step, I placed the test specimens on the rollers in the middle of the cooling equipment. Then I cooled the test pieces to the desired temperature. I kept the temperature for 15 minutes so that the test body cooled down completely. I measured the temperature with two type K thermocouples. During the test, the displacement speed was 0.5 mm/min. I plotted the change in force as a function of the displacement of the load line (LLD). The measurement results can be seen in Table 20-22.

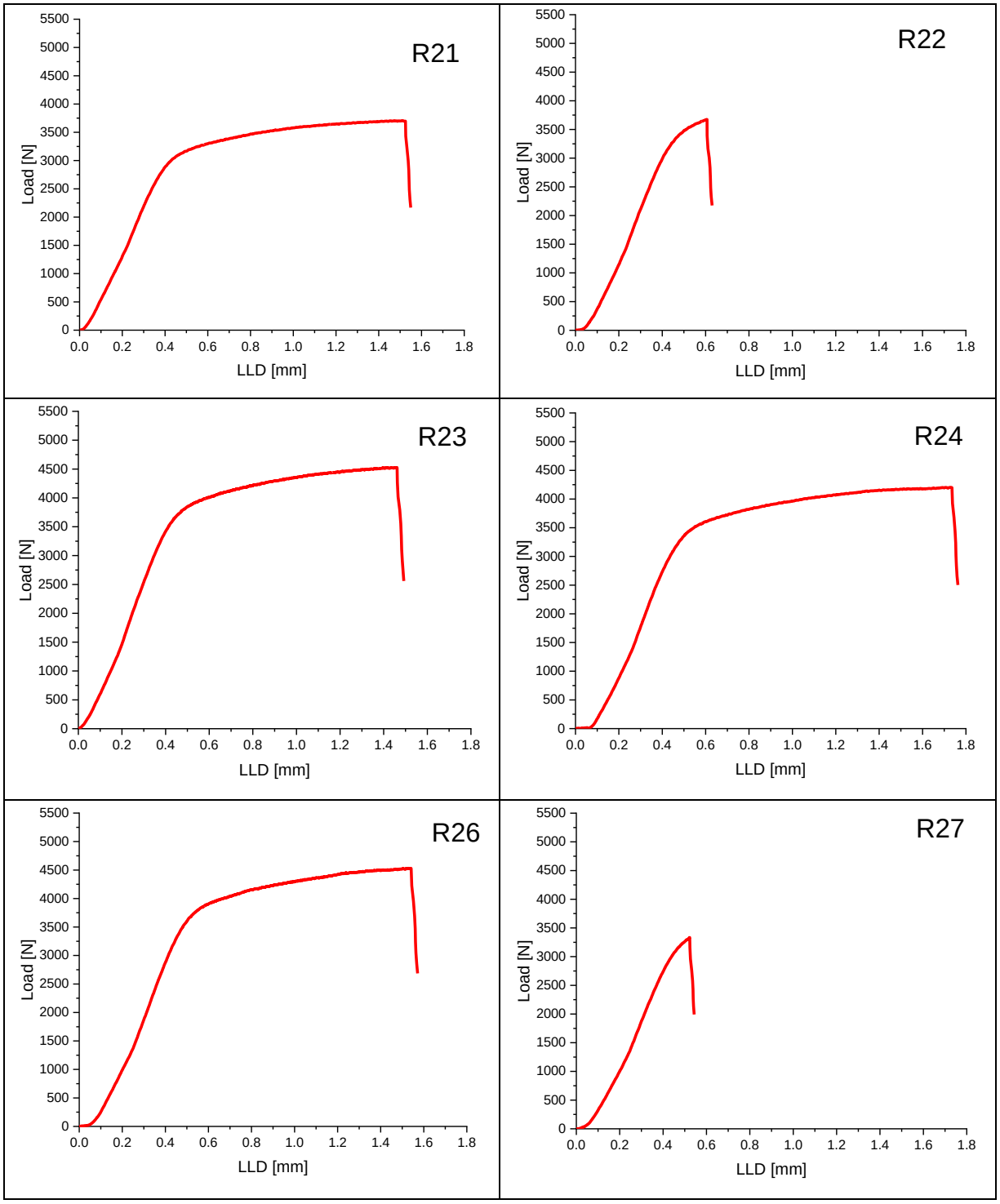

Figure 20. LLD vs load curves

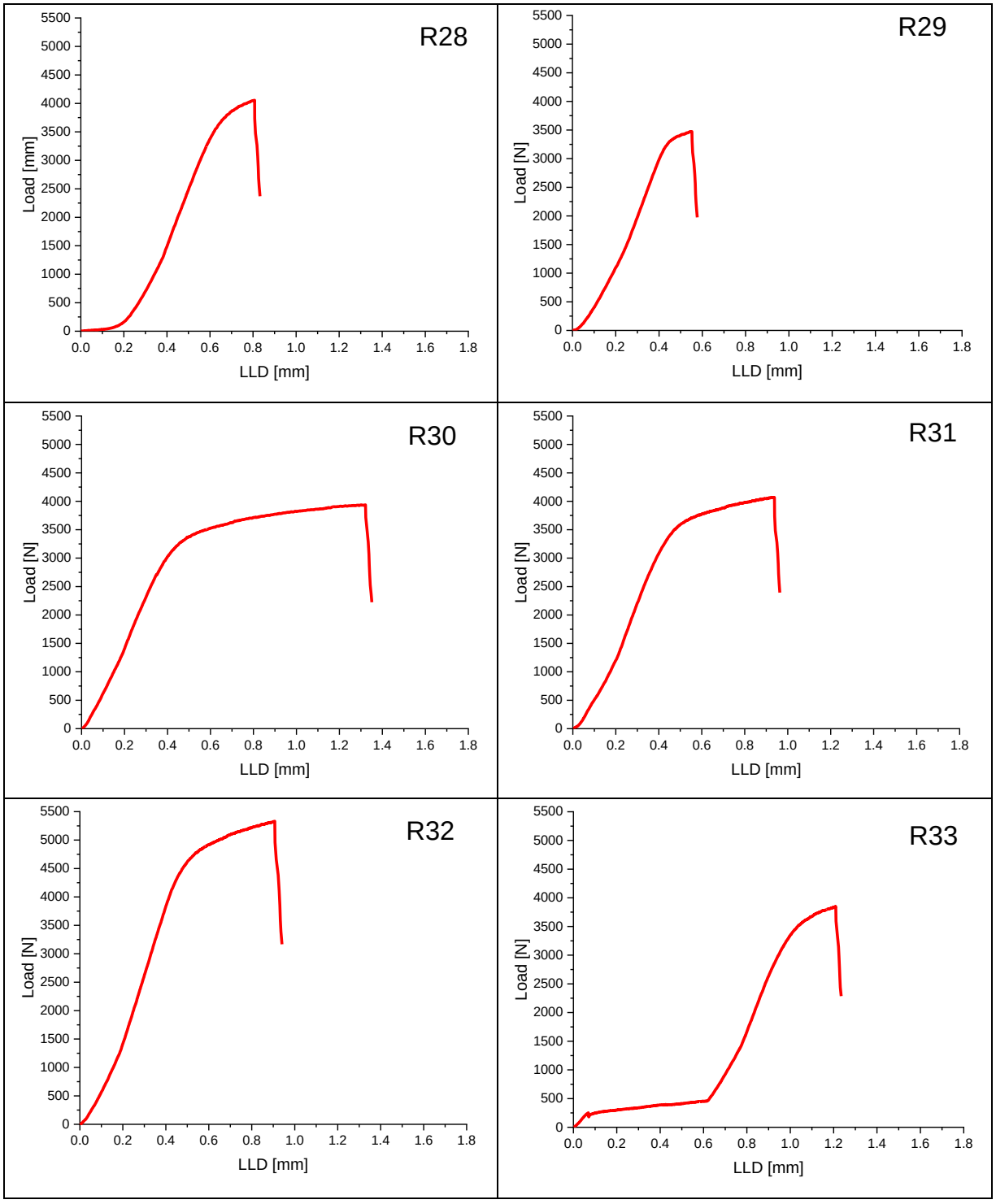

Figure 21. LLD vs load curves

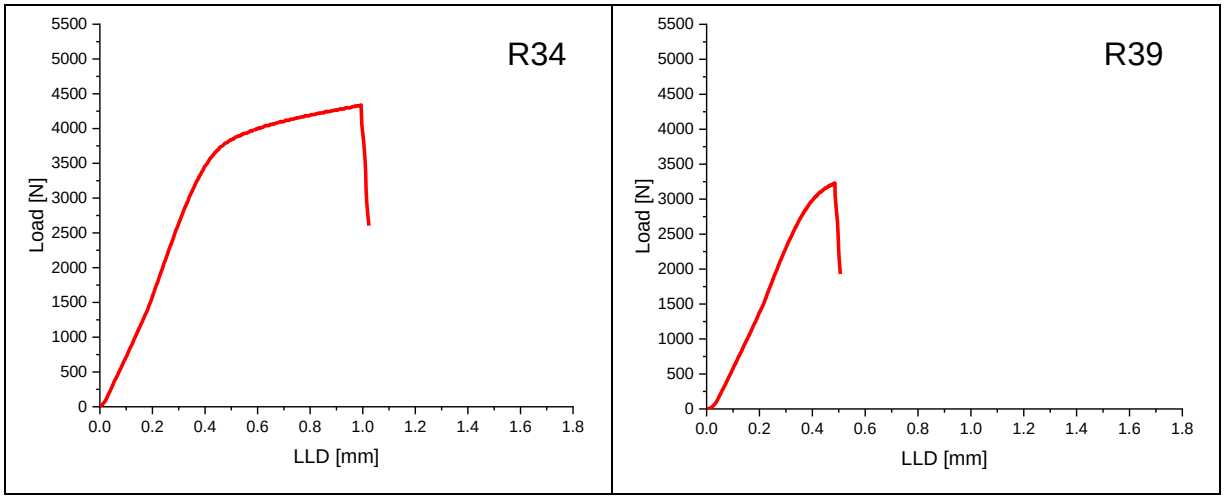

Figure 22. LLD vs load curves

From the measured curves, I determined the parameters (Table 9.) necessary for the evaluation:

- load line displacement (LLD) in mm,
- P: magnitude of the loading force at the moment of fracture,
- C_0: reciprocal of the initial slope in the linear-elastic range,
- A: area under force versus displacement test records (a measure of work done),
- A_e: area of the elastic deformation,
- A_p: area of the plastic deformation (Figure 23.).

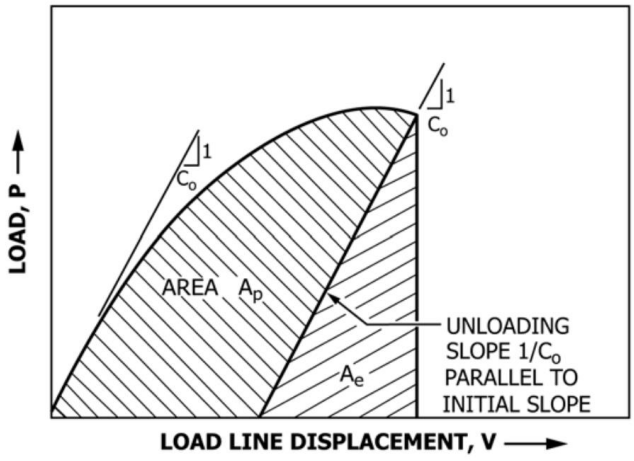

Figure 23. Diagram of the parameters of the area under the curve

code	T [°C]	W [mm]	B [mm]	a_0 [mm]	b_0 [mm]	P [N]	c_0	A [mmN]	A_e [mmN]	A_p [mmN]
R21	-70	10.00	5.00	4.96	5.04	3705.5	$1.25x10^{-4}$	4545.0	855.5	3689.5
R22	-80	9.99	5.00	4.67	5.32	3674.1	$1.08x10^{-4}$	1279.3	729.9	549.4
R23	-75	9.98	5.00	4.49	5.49	4526.3	$9.91x10^{-5}$	5235.6	1015.5	4220.1
R24	-80	9.99	5.00	4.78	5.21	4203.9	$1.08x10^{-4}$	5715.0	953.5	4761.4
R26	-85	9.98	4.98	4.5	5.48	4532.2	$1.11x10^{-4}$	5316.7	1140.9	4175.8
R27	-90	9.98	4.99	4.9	5.08	3333.3	$1.21x10^{-4}$	882.5	674.1	208.3
R28	-85	9.98	5.00	4.37	5.61	4056.0	$1.03x10^{-4}$	1519.0	848.7	670.3
R29	-85	9.99	5.00	4.87	5.12	3473.3	$1.03x10^{-4}$	1060.1	619.0	441.2
R30	-85	10.00	4.99	5.02	4.98	3937.2	$1.16x10^{-4}$	4071.4	901.7	3169.8
R31	-85	10.00	4.99	4.67	5.33	4069.9	$1.01x10^{-4}$	2659.1	835.9	1823.2
R32	-85	10.00	5.00	3.75	6.25	5331.3	$8.22x10^{-5}$	3272.9	1168.1	2104.8
R33	-85	10.00	4.99	4.73	5.27	3847.4	$1.06x10^{-4}$	1747.5	783.8	963.7
R34	-85	9.99	5.01	4.6	5.39	4339.9	$9.66x10^{-5}$	3175.5	909.3	2266.2
R39	-80	9.99	5.00	4.88	5.11	3231.0	$1.16x10^{-4}$	891.1	607.8	283.3

Table 9. Determined parameters

Sample R32 is not included in the further evaluation, because the depth of fatigue was too small. During the measurement of the R33 specimen, the tool moved, probably due to icing, thus giving an incorrect curve. This sample was also excluded.

Based on what was described in chapter 4.2.2.3, I processed the measurement data. The calculations are very long and difficult to grasp. To eliminate this, I developed a calculation program in Excel. The results are contained in table 10. The results were then censored and plotted on the fracture toughness trend curve (Figure 24.). The temperature value corresponding to 100 $MPam^{1/2}$ can be read from here.

Specimen name	Non Adjusted K_{Jc} [$MPam^{1/2}$]
R21	202.93
R22	107.65
R23	270.18
R24	293.16
R26	267.11
R27	87.16
R28	123.99
R29	101.91
R30	249.39
R31	167.40
R32	180.21
R33	128.02
R34	203.56
R39	97.79

Table 10. Non censored K_{JC} values

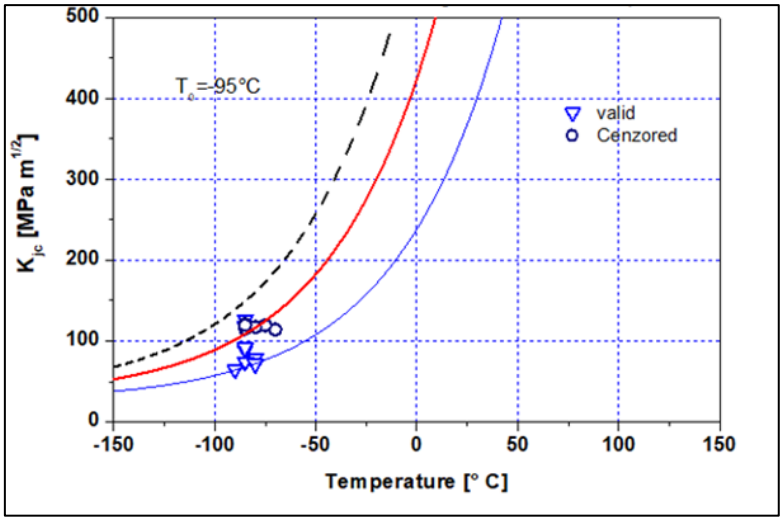

Figure 24. Master curve

The calculated T_0 = -95 °C. This result is the same as the data found in the literature (-94 °C) (REVKA ET AL., 2010).

Optical investigation

I performed optical and electron microscopic analyzes on the fracture surface of each sample (see in Annex). Micrometer scale precipitates were visible in several samples. Only on two sample (R30) was it observed that the size of the precipitates reached several tens of micrometers (Figure 25.). According to the EDS analysis performed on the fracture surface, these spherical precipitates have a Fe-Mo-C and the grey-black precipitates (Figure 26.) Fe-C composition (R33).

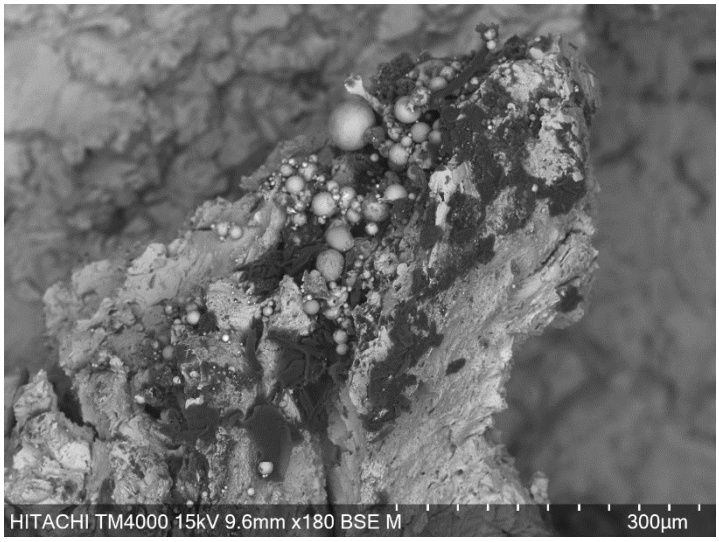

Figure 25. Precipitates in the sample R30

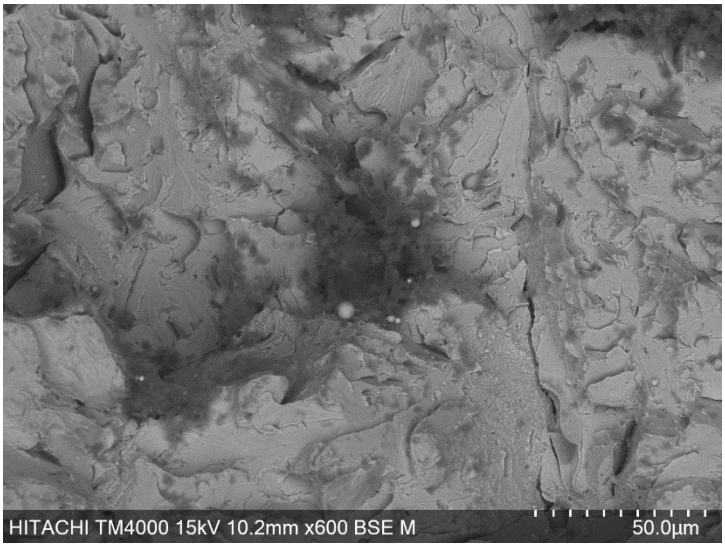

Figure 26. Precipitates in the sample R33

With the help of fractographic analyses, the ductile-brittle transition can be clearly traced (Figure 28.)

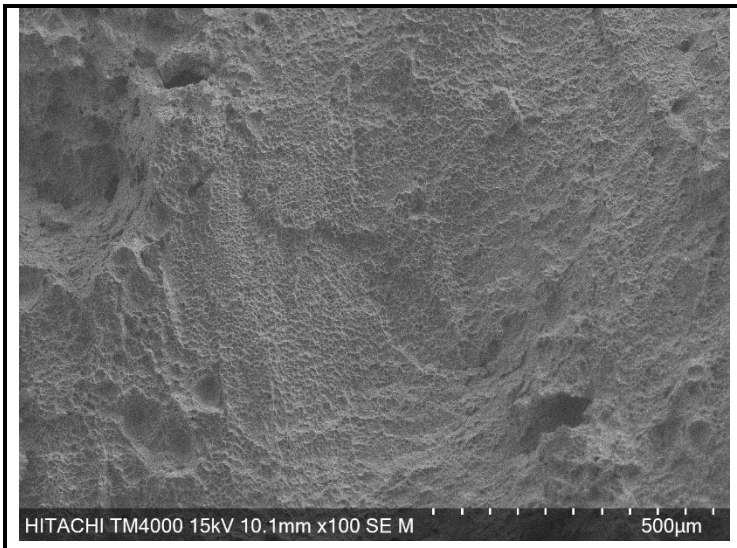

R40 RT

Fully ductile

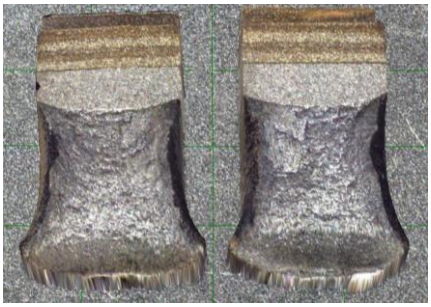

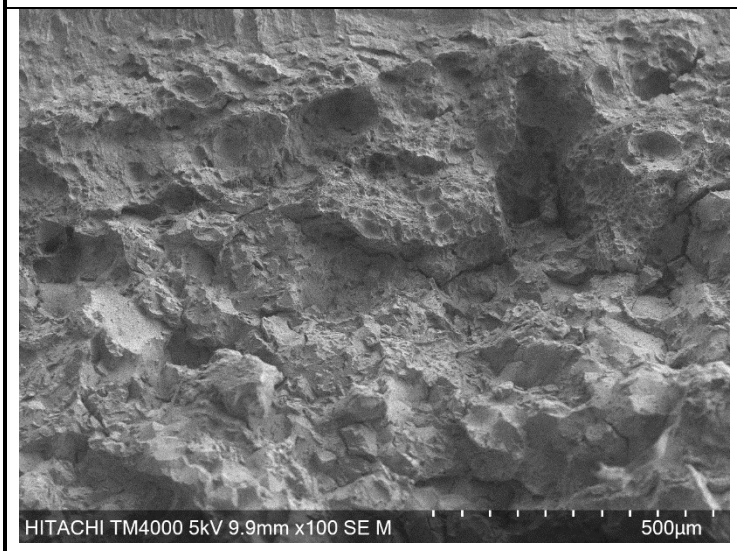

R21 -70°C

Ductile-brittle

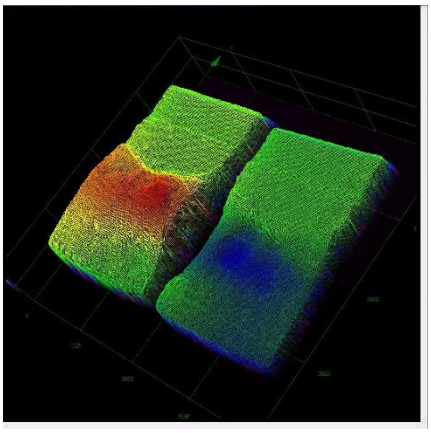

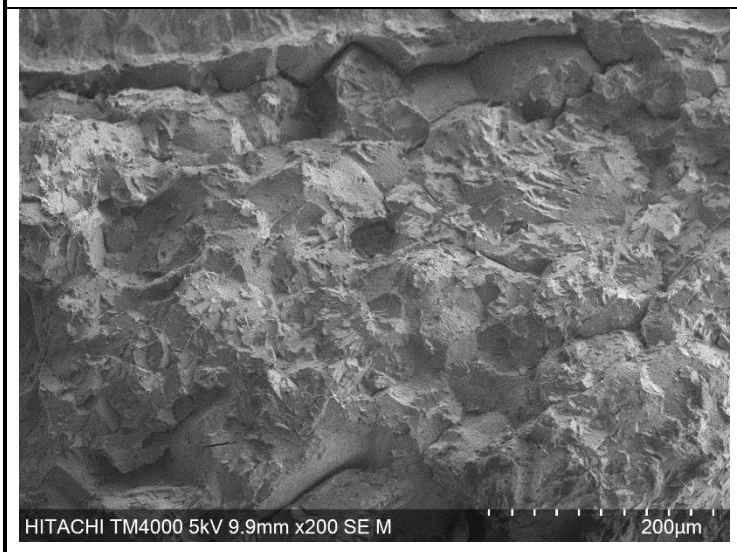

R27 -90°C

Brittle

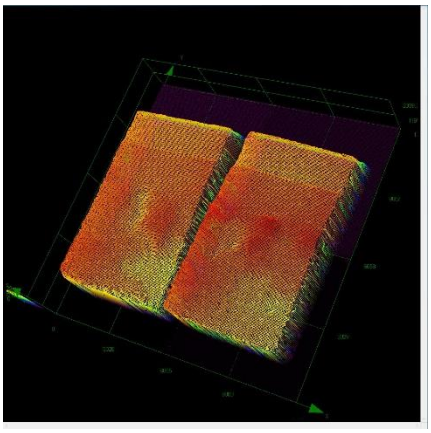

Figure 28. Ductile-brittle transition on the fracture surface

6. ESTIMATED TRANSITION TEMPERATURE

Based on accumulated operational experience and mechanical tests, it is possible to be determined the shift of the DBTT by so-called chemical formulas. Separate formulas have been developed for both the weld material and the base material. Based on the formula (Eq.16.), the embrittlement trend can be calculated. Of course, this is just an estimate. The formulas are the results of statistical analyses. The real extent of the DBTT shift is always determined from the mechanical tests performed on the surveillance specimens (Gillemot et al., 2023).

$$\Delta T = 8.37 F^{0.43} , \tag{16}$$

Where:

F = neutron fluence

Based on the equation, I plotted the value of the expected DBTT as a function of fluence (Figure 28.). I determined the value of the DBTT in the 30th and 60th years of operation, if the neutron spectrum is integrated above 0.5 and 1 MeV, respectively (Table 11.). The standard deviation is 21.6 °C.

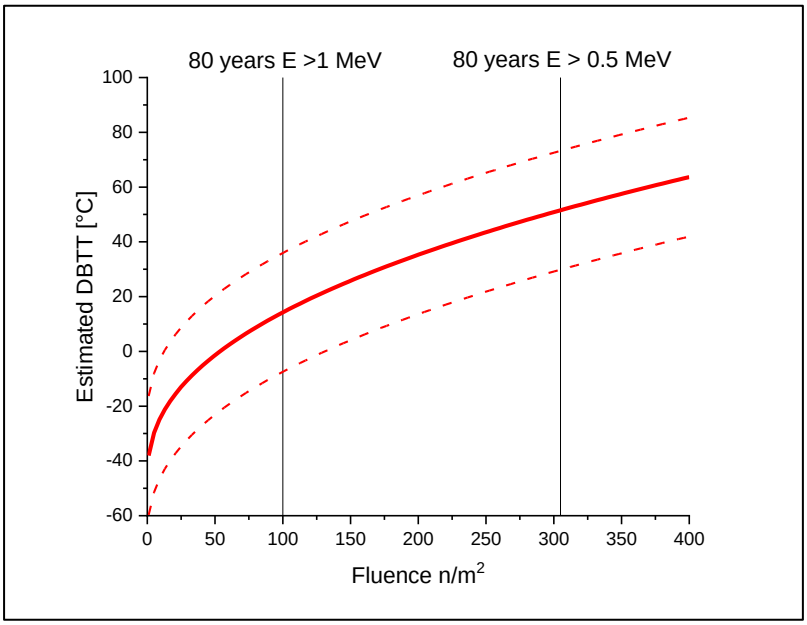

Figure 28. Trend curve of the 15H2NMFA steel

	E > 1 MeV	E > 0.5 MeV
30 years operation	-6.6 °C	17.8
60 years operation	7.2 °C	40.1

Table 11. Estimated transition temperature

7. CONCLUSION

Regarding the microstructure of the examined material, it is a ferrite-pearlite steel with grain size less than 100 µm. It does not contain gas bubbles, only a small amount of inclusions. Most of the inclusions are MnS, the size of which varies between a few µm and 30 µm.
In terms of its mechanical properties, it meets the manufacturer's specification in all respects. The results of the tensile tests performed at room temperature far exceed expectations. The material showed fully plastic behavior (Table 12.).

	$R_{p0.2}$ [MPa]	R_m [MPa]	A %	Z %
Minimum value	441	549	15	55
Measured value	591	692	22	70

Table 12. Comparison table of the tensile test

Based on the Charpy fracture mechanics results, I determined that the transition temperature value for 41 J is -46.4 °C, compared to the minimum value of -25 °C.

New reactor vessel monitoring programs require the determination of the T_0 reference temperature value. This is -95 °C as a result of the series of measurements and calculations shown above.

Taking into account the trend curve calculations, this steel alloy is suitable for making a long-term reactor vessel operating for 60-80 years. This is only an estimate based on previous measurement results. The actual degree of embrittlement will be shown by the measurement results of the survillance specimens.

ACKNOWLEDGMENTS

First of all, I would like to thank my supervisor Dr. Ferenc Gillemot. In addition to helping the completion of the work with his advice, he introduced me to the mysteries of a completely new scientific field for me, for which I am very grateful.

I would like to thank my consultant Prof. Dr. Jenő Gubicza for helping the completion of the work with his comments.

I am grateful to my colleagues – Márta Horváth, Balázs Hargitai, Andor Kristóf Csikós, Zoltán Hózer, Ildikó Szenthe - for continuously helping me with my work.

And last but not least, I thank my family for supporting me all the way.

8. REFERENCES

[1] ASM Metals Handbook, Ninth Edition: "Metallography and Microstructures", American Society for Metals

[2] ASTM E3 standard (Standard Guide for Preparation of Metallographic Specimens)

[3] ASTM E8/E8M standard (Standard Test Methods for Tension Testing of Metallic Materials)

[4] ASTM E23 standard (Standard Test Methods for Notched Bar Impact Testing of Metallic Materials)

[5] ASTM E185 standard Standard Practice for Design of Surveillance Programs for Light-Water Moderated Nuclear Power Reactor Vessels

[6] ASTM E407 standard (Standard Practice for Microetching Metals and Alloys)

[7] ASTM E1921 standard (Standard Test Method for Determination of Reference Temperature, T0, for Ferritic Steels in the Transition Range)

[8] Jiri Brynda, Vladimir Cerny, Radek Konop (2002): *"VVER REACTOR PRESSURE VESSEL MATERIALS DATABASE AND MONITORING OF AGEING AND LIFETIME EVALUATION"*, AFEING Varna

[9] Jiri Brynda, Jozef Hogel , Milan Brumovsky (2003): *"Surveillance Specimen Programmes for WWER Reactor Vessels in the Czech Republic",* Transactions of the 17th International Conference on Structural Mechanics in Reactor Technology (SMiRT 17) Prague, Czech Republic

[10] Dmitry Erak , Boris Gurovich , Denis Zhurko , Evgenia Kuleshova , Anna Chernobaeva , Valentina Papina , Oleg Zabusov , Anatoly Hodan (2015) "*IMPROVEMENT OF RADIATION EMBRITTLEMENT DEPENDENCES FOR VVER-1000 PRESSURE VESSEL MATERIALS ON SERVICE-LIFE EXTENSION*" SMiRT-23 Manchester, United Kingdom, Division: Mechanics of Materials

[11] Gillemot, Horváth (2010): "*MASTER CURVE AND ITS APPLICATION IN THE NUCLEAR INDUSTRY*" Anyagvizsgálók lapja

[12] Ferenc Gillemot, Dávid Cinger, Ildikó Szenthe, Márta Horváth, Szilvia Móritz (2023): "*Radiation Embrittlement Surveillance and Trend Evaluation in Hungary*" under publication

[13] Jastrzebski, D. (1959): "Nature and Properties of Engineering Materials" (Wiley International ed.). John Wiley & Sons, Inc.

[14] Kim Wallin (2016): "*Subsized CVN Specimen Conversion Methodology*" Procedia Structural Integrity

[15] Kurishita H, Kayano H, Narui M, Yamazaki M, Kano Y, Shibahara I (1993). *"Effects of V-notch dimensions on Charpy impact test results for differently sized miniature specimens of ferritic steel*". Materials Transactions - JIM. Japan Institute of Metals

[16] Joseph Maciejewski (2015): *"The Effects of Sulfide Inclusions on Mechanical Properties and Failures of Steel Components"*, Journal of Failure Analysis and Prevention

[17] Mathurt KK, Needleman A, Tvergaard V (May 1994). "*3D analysis of failure modes in the Charpy impact test*". Modelling and Simulation in Materials Science and Engineering

[18] Meyers Marc A; Chawla Krishan Kumar (1998): "*Mechanical Behaviors of Materials"* Prentice Hall

[19] Donald E. McCabe, John G. Merkle, and Kim Wallin (2005): "*An Introduction to the Development and Use of the Master Curve Method*" ASTM Stock Number: MNL52 INTERNATIONAL Standards Worldwide ASTM International

[20] Mills NJ (1976): "*The mechanism of brittle fracture in notched impact tests on polycarbonate*". Journal of Materials Science

[21] R. Novoreftov (2010): Российский дизайн «Атомного окна» в Европу *Russian design of the "Atomic Window" to Europe*, Energyland.info

[22] OAH 3.18. A VVER-440/213 reaktortartály ridegtöréssel szembeni biztonságának értékelése normál üzem, szilárdsági nyomáspróba, nyomás alatti hőütés (PTS) és nem várt üzemi események esetén

[23] Igor Orynyak, Maksym Zarazovskii, Andrii Bogdan (2013): "Determination of the Transition Temperature Scatter Using the Charpy Data Scatter", ASME 2013 Pressure Vessels and Piping Conference

[24] Oldekop, W. (1982), *"Electricity and Heat from Thermal Nuclear Reactors"*, Primary Energy, Berlin, Heidelberg: Springer Berlin Heidelberg

[25] V. M. Revka, E. U. Grynik, and L. I. Chyrko (2010): "*The Use of Master Curve Method for Statistical Re-Evaluation of Surveillance Test Data for WWER-1000 Reactor Pressure Vessels*", Strength of materials

[26] Székely Levente Csaba (2021): "*A hőkezelés hatása a reaktortartály plattírozással felrakott rétegének szövetszerkezetére*", Bányászati és kohászati lapok, Kohászat

[27] B. T. Timofeev, G. P. Karzov (2005): "*Assessment of the WWER440/V-213 reactor condition*", International Journal of Pressure Vessels and Piping

[28] B.T. Timofeev, G.P. Karzov (2006): "*Assessment of the WWER-1000 reactor condition*", International Journal of Pressure Vessels and Piping

[29] André Luiz Vasconcellos da Costa e Silva (2018): *"Non-metallic inclusions in steels – origin and control"*, Journal of Material Research and Technology

[30] Van Vliet, Krystyn J. (2006); "*Mechanical Behavior of Materials*"

Figures:

https://www.911metallurgist.com/charpy-impact-machine/

https://yenaengineering.nl/ductile-brittle-transition-temperature-and-impact-energy-tests/

https://world-nuclear.org/information-library/nuclear-fuel-cycle/nuclear-power reactors/nuclear-power-reactors.aspx

9. ANNEX

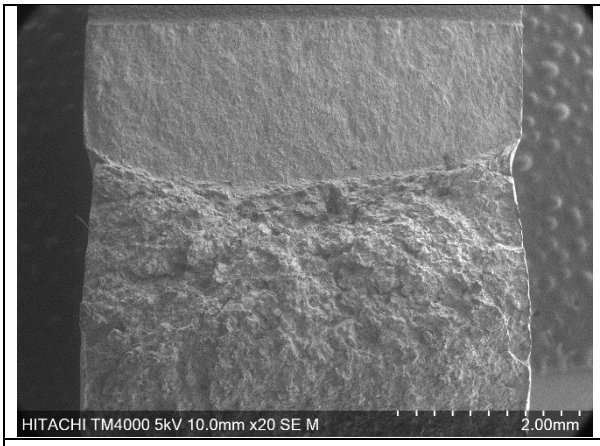

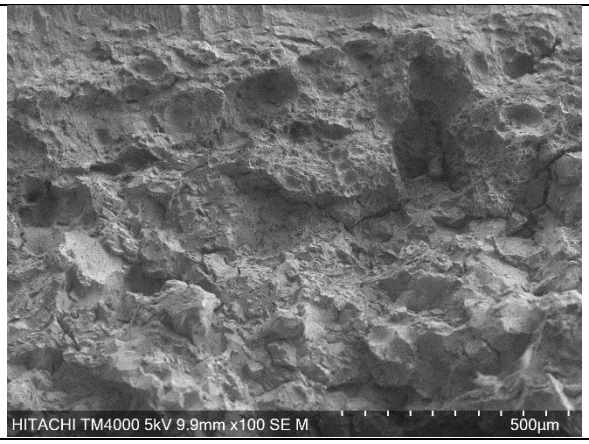

Electron microscopic pictures, sample: R21

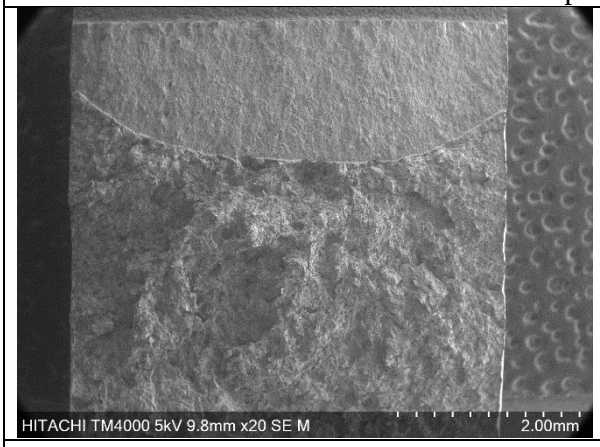

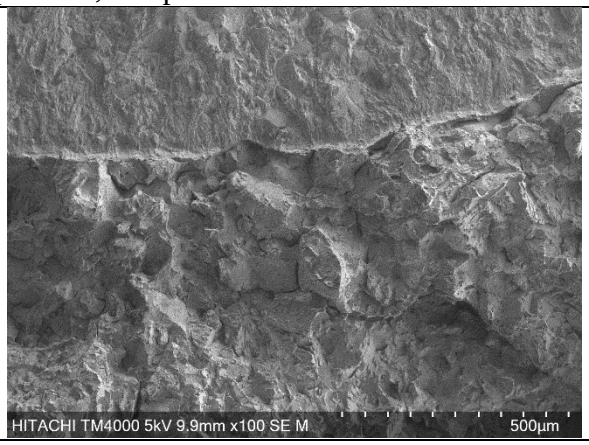

Electron microscopic pictures, sample: R22

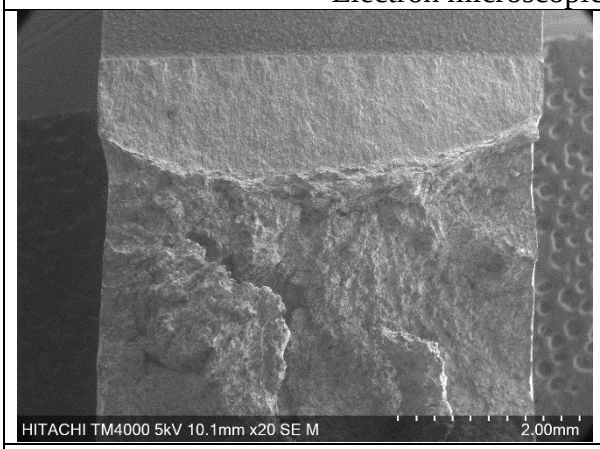

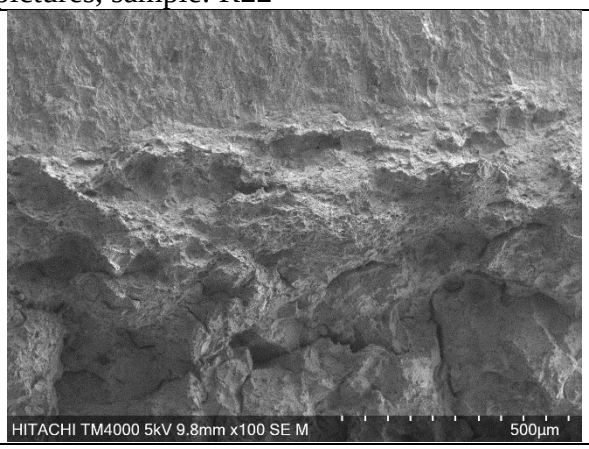

Electron microscopic pictures, sample: R23

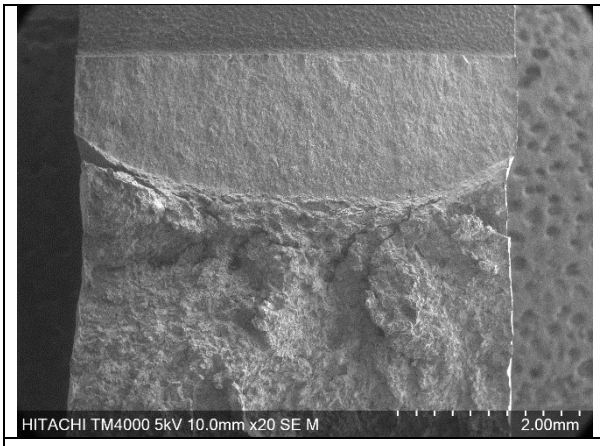

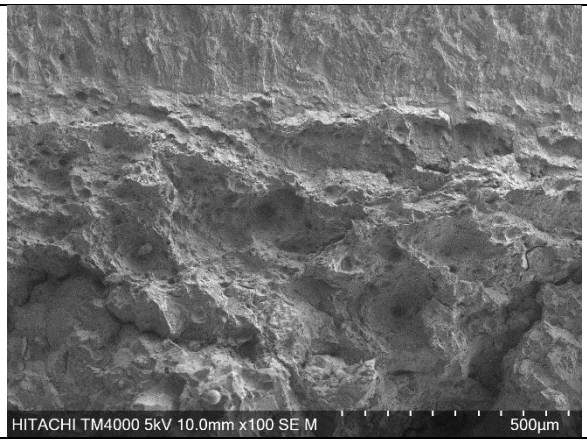

Electron microscopic pictures, sample: R24

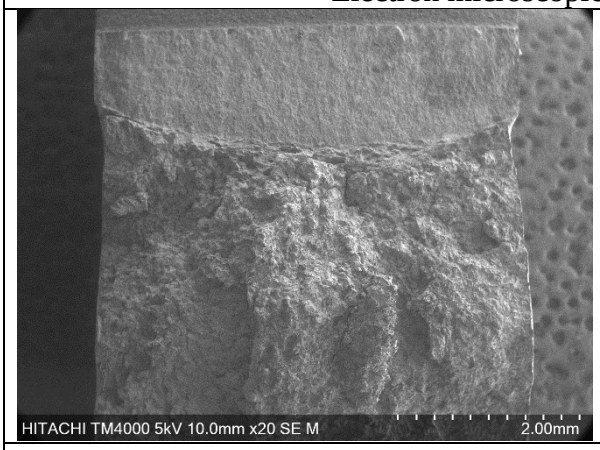

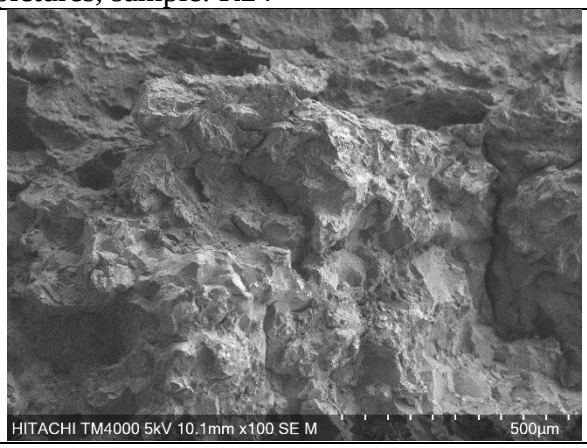

Electron microscopic pictures, sample: R26

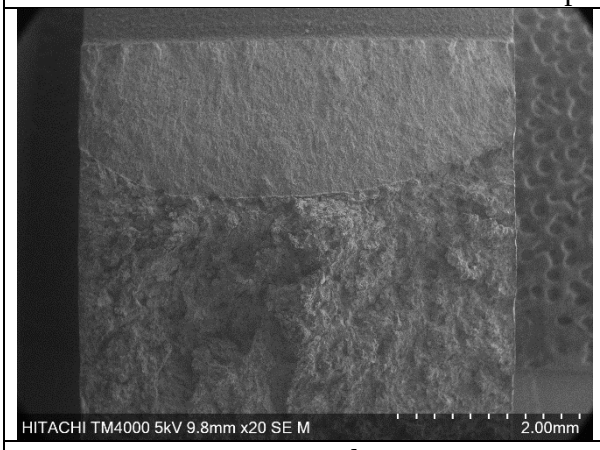

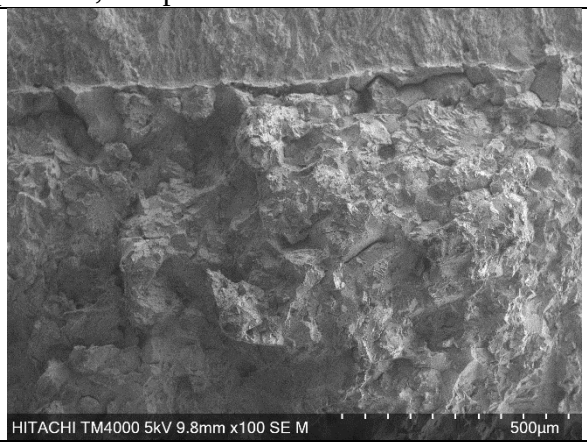

Electron microscopic pictures, sample: R27

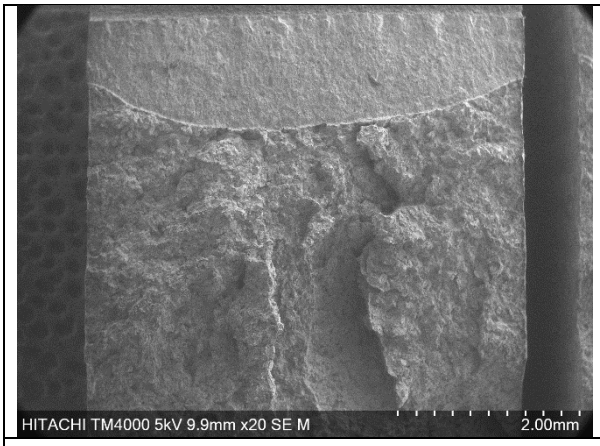

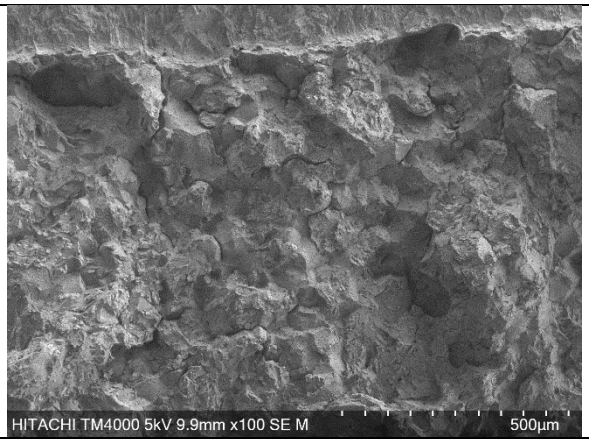

Electron microscopic pictures, sample: R28

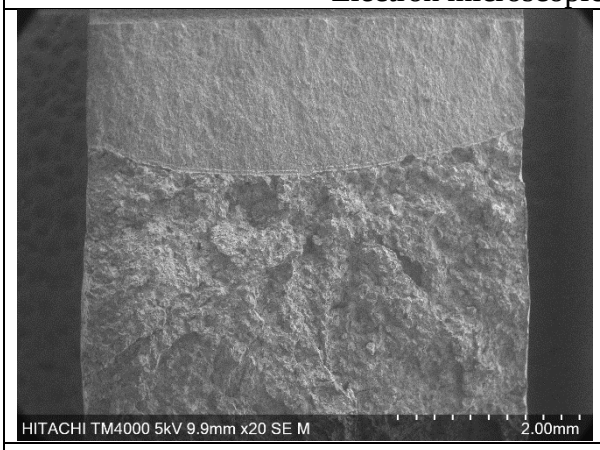

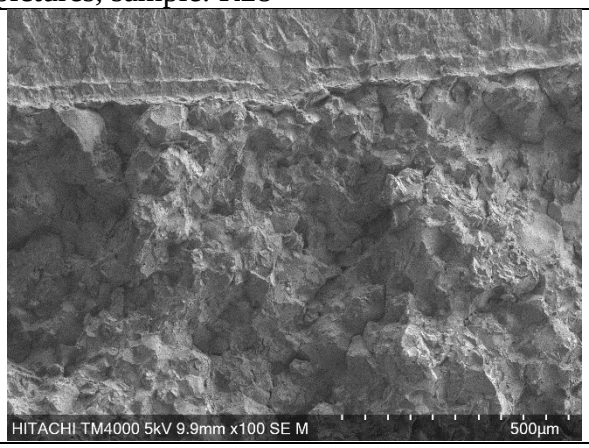

Electron microscopic pictures, sample: R29

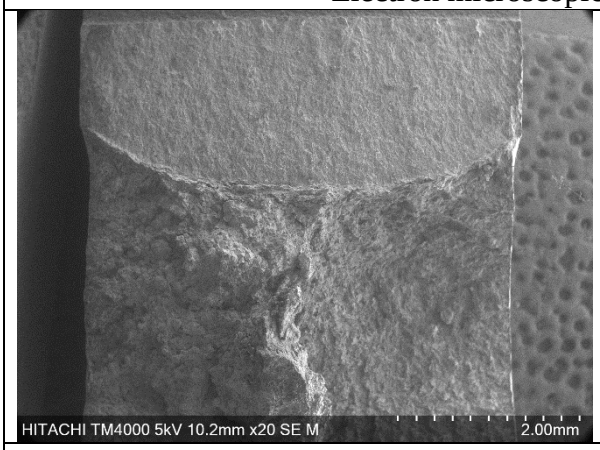

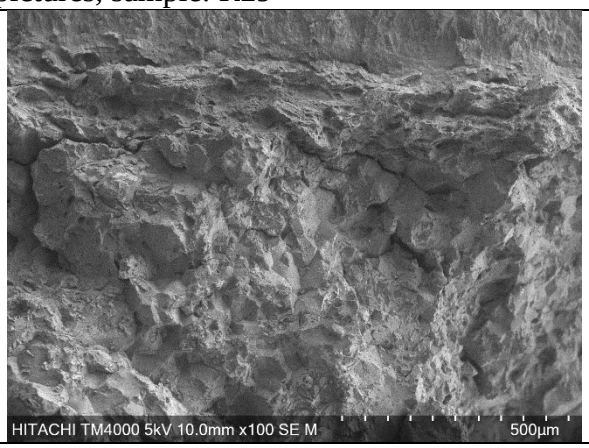

Electron microscopic pictures, sample: R30

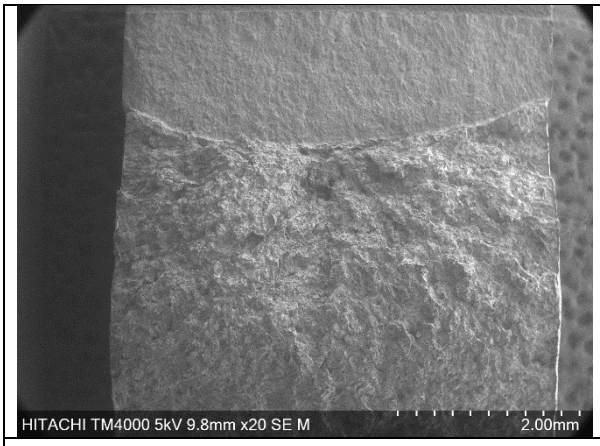

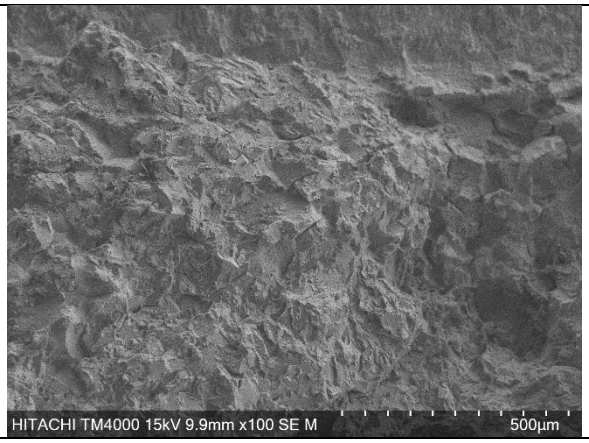

Electron microscopic pictures, sample: R31

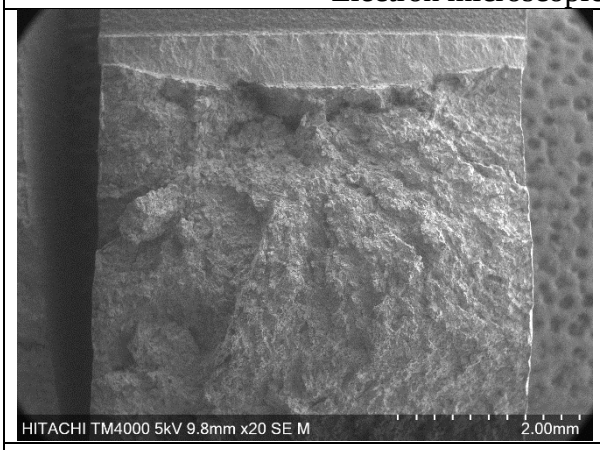

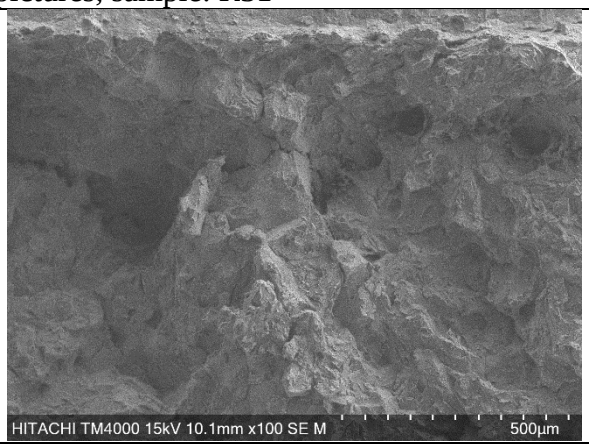

Electron microscopic pictures, sample: R32

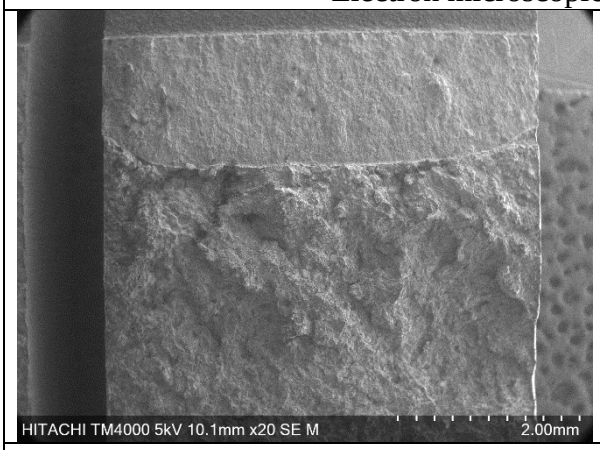

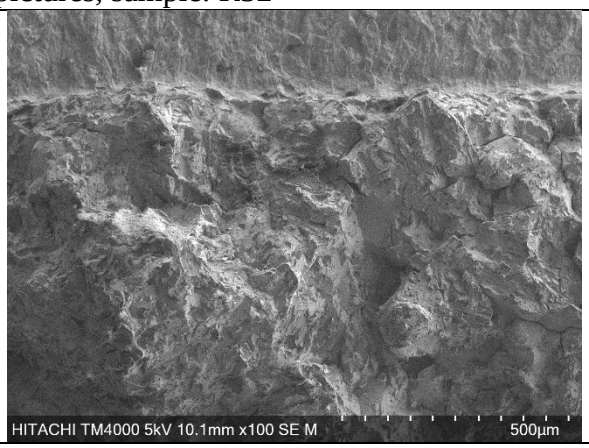

Electron microscopic pictures, sample: R33

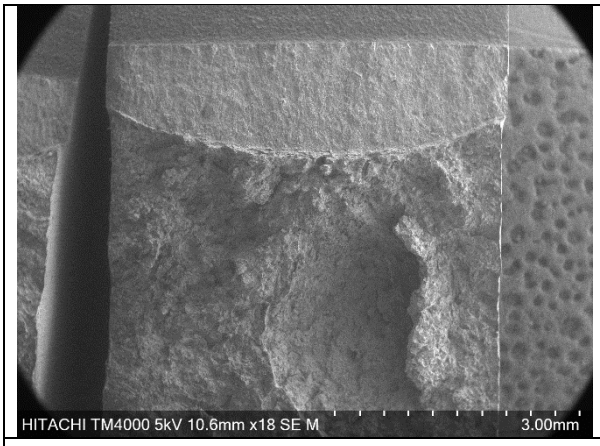

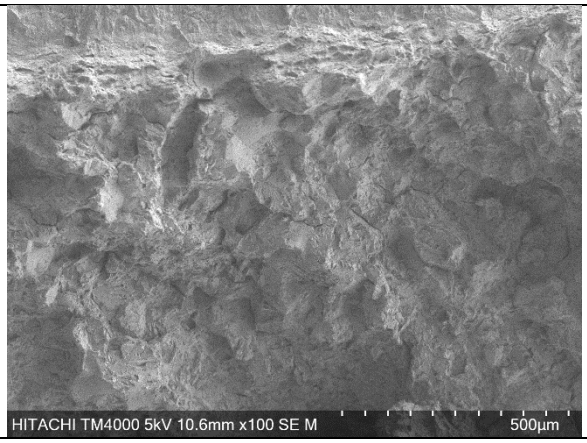

Electron microscopic pictures, sample: R34

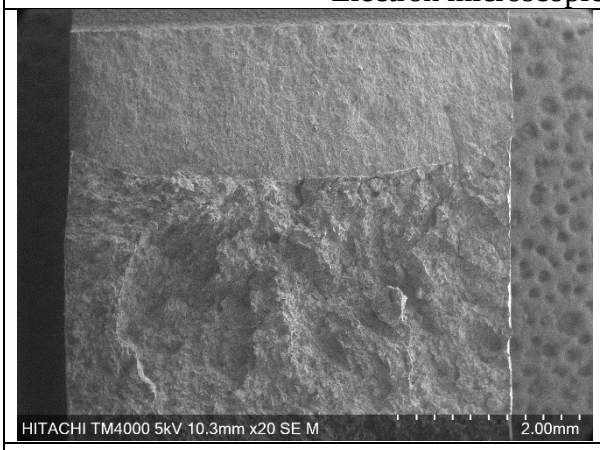

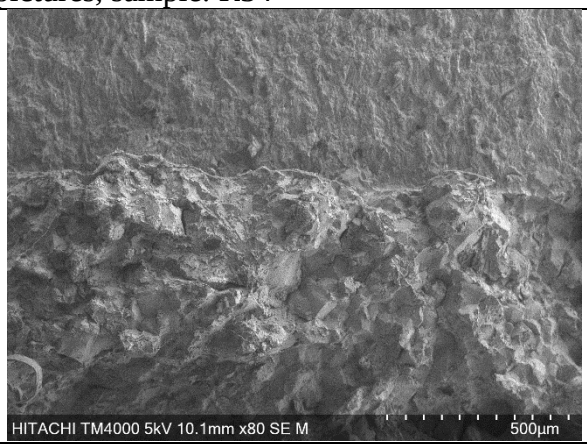

Electron microscopic pictures, sample: R39

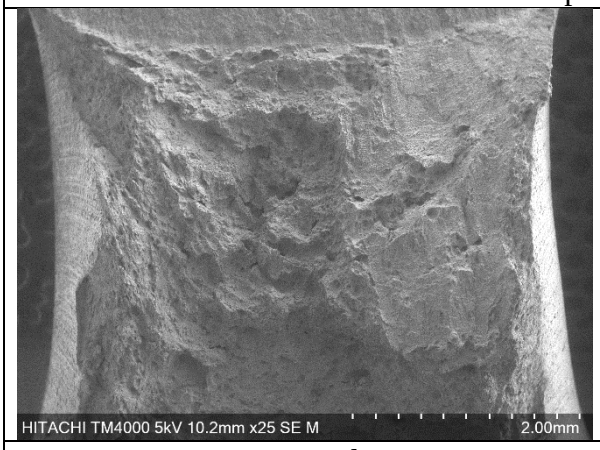

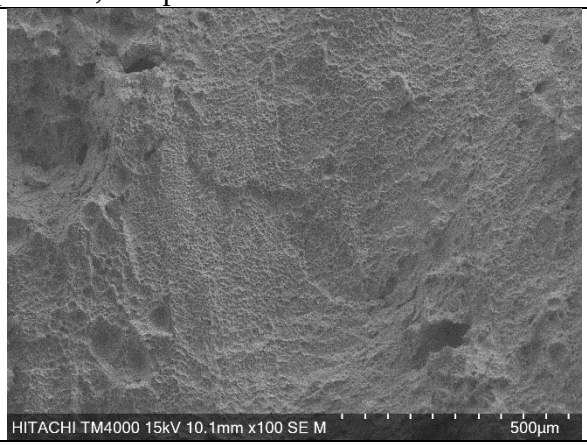

Electron microscopic pictures, sample: R40

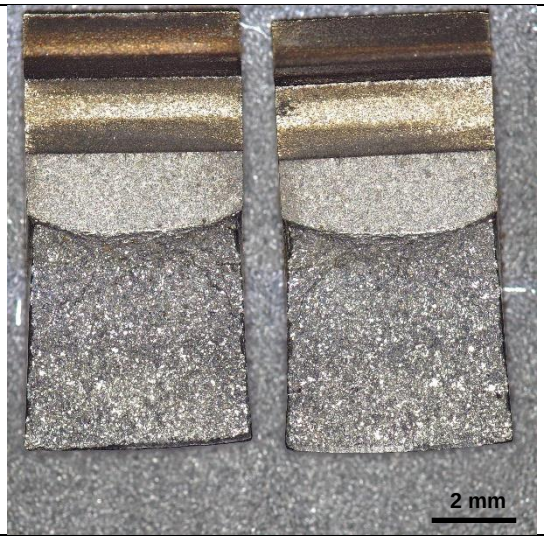

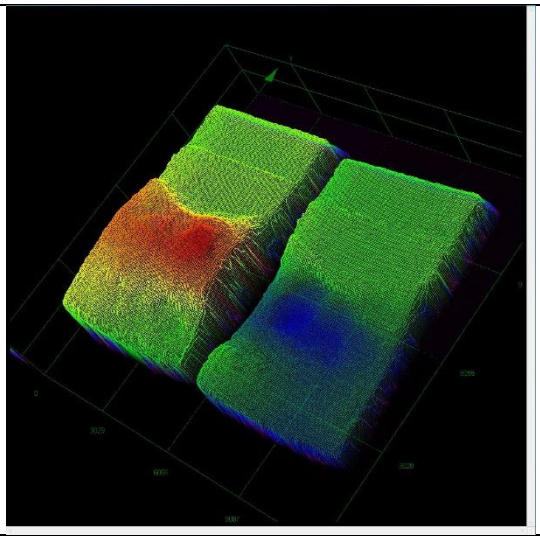

Optical microscopic and height-contrast pictures: R21

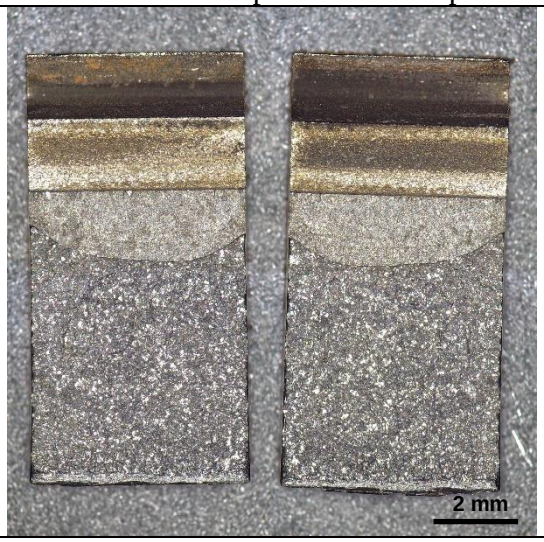

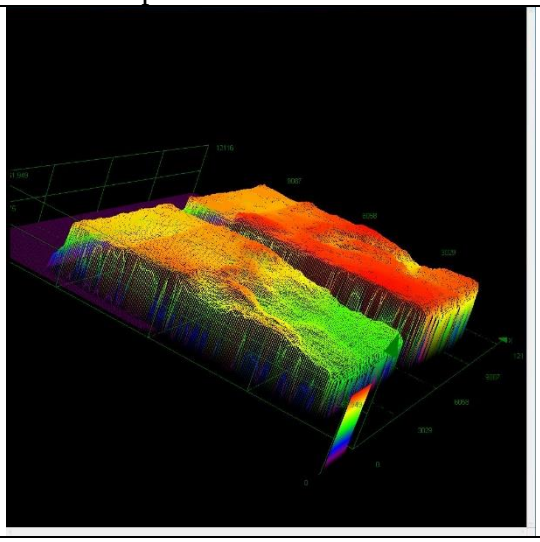

Optical microscopic and height-contrast pictures: R22

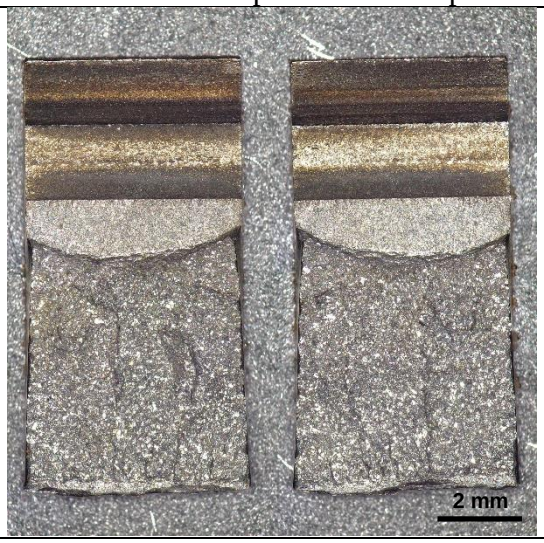

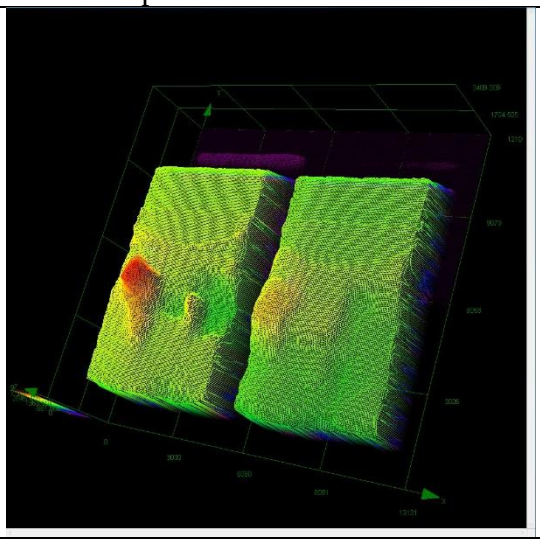

Optical microscopic and height-contrast pictures: R23

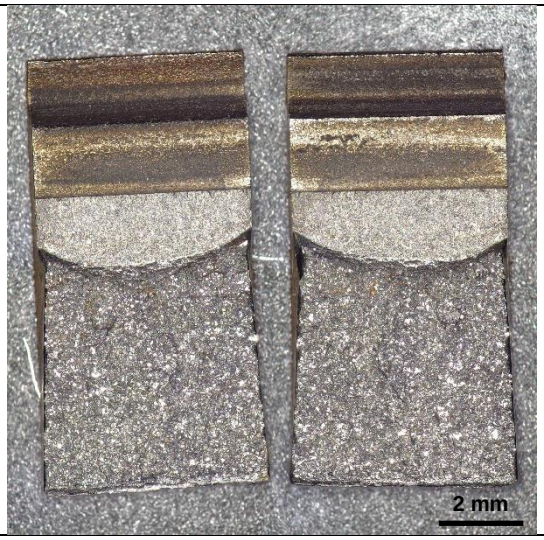

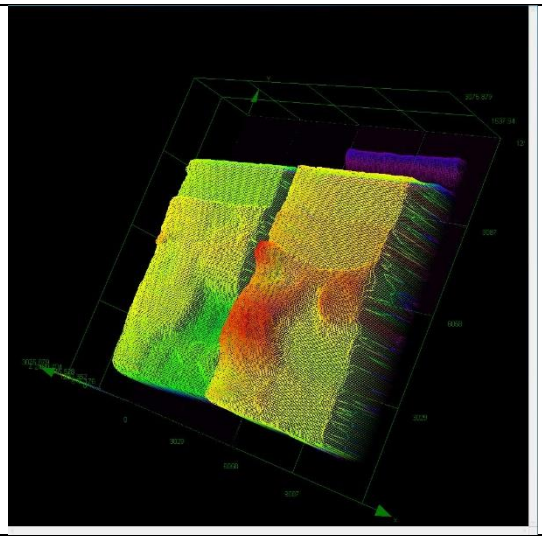

Optical microscopic and height-contrast pictures: R24

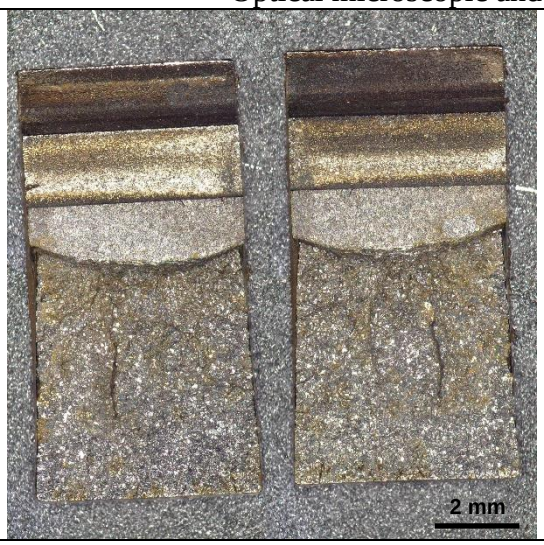

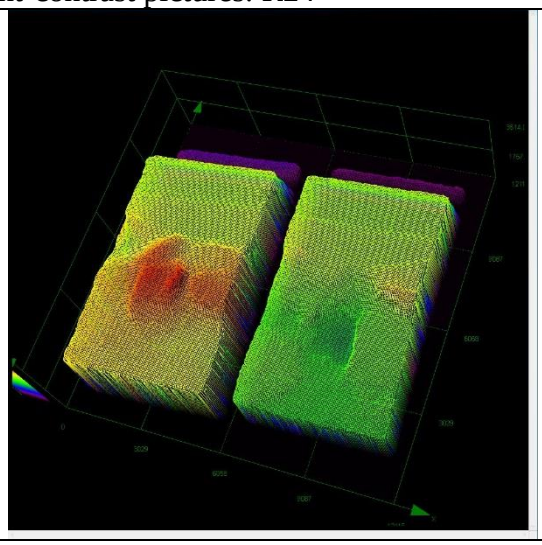

Optical microscopic and height-contrast pictures: R26

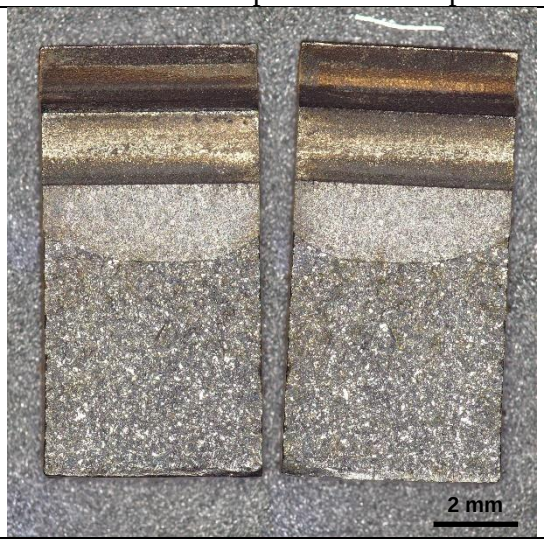

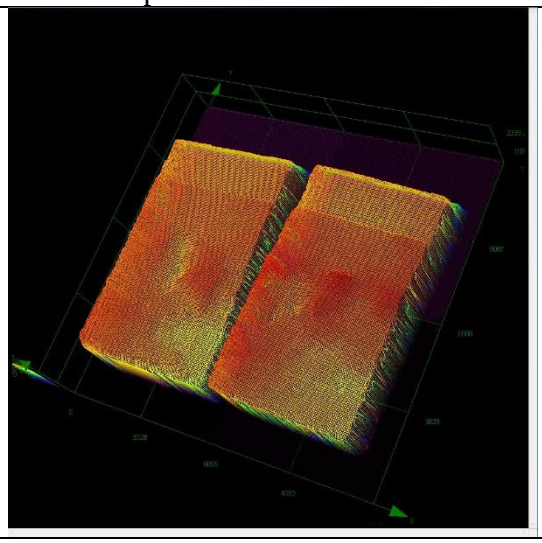

Optical microscopic and height-contrast pictures: R27

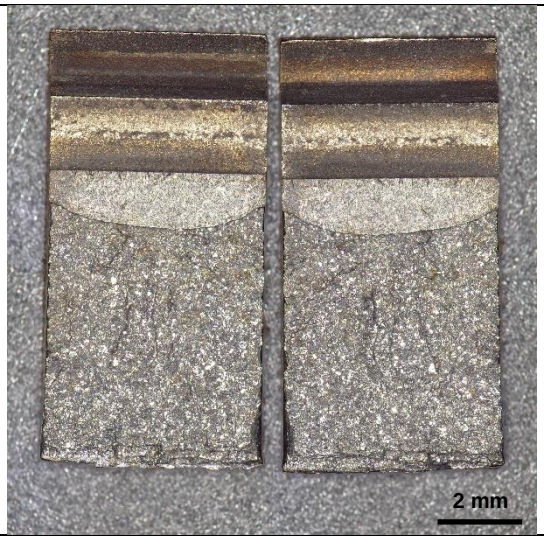

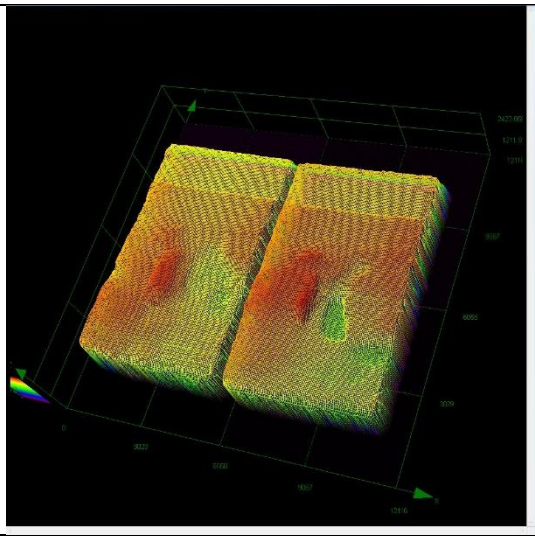

Optical microscopic and height-contrast pictures: R28

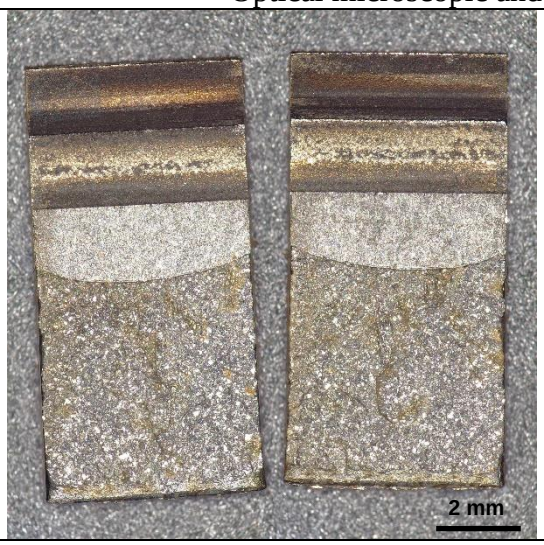

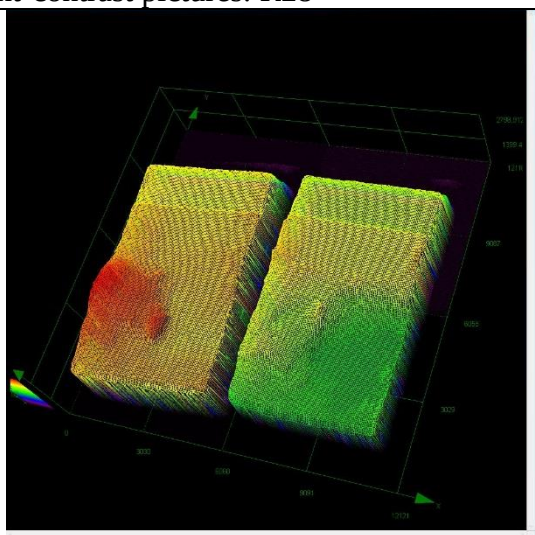

Optical microscopic and height-contrast pictures: R29

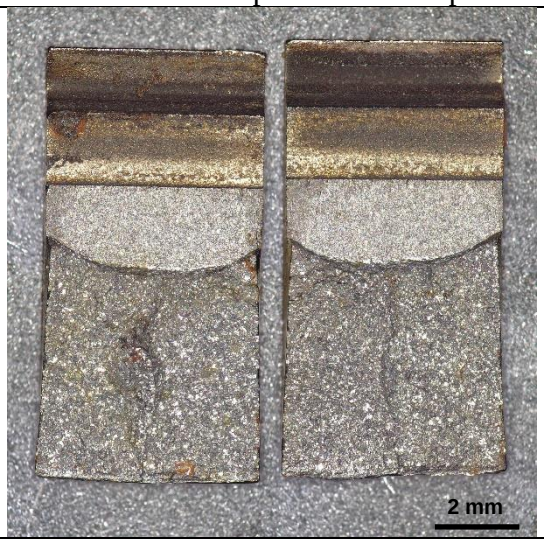

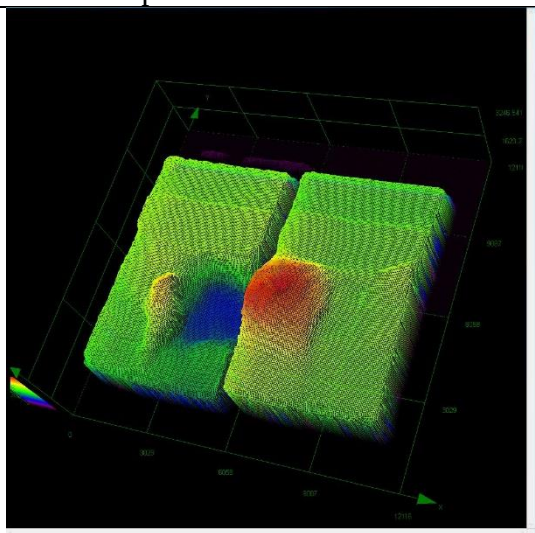

Optical microscopic and height-contrast pictures: R30

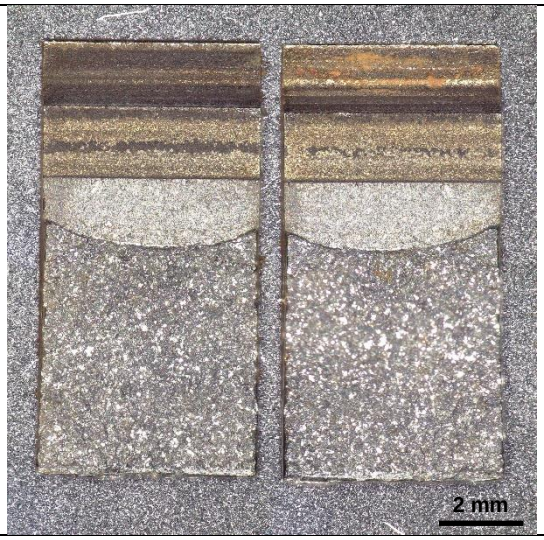

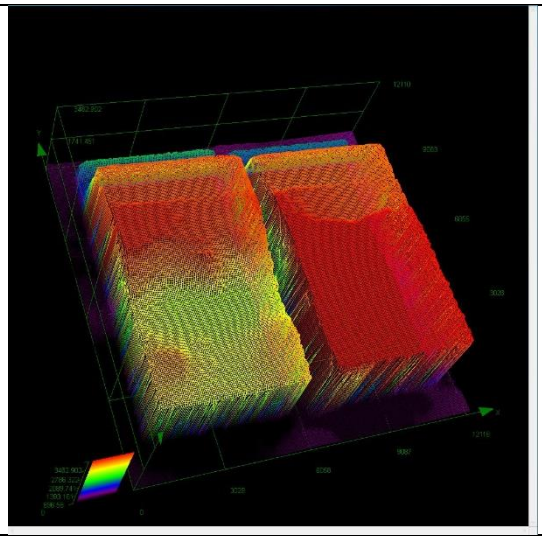

Optical microscopic and height-contrast pictures: R31

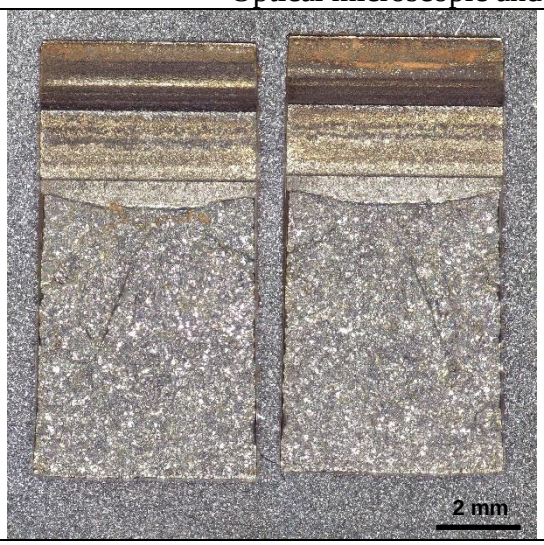

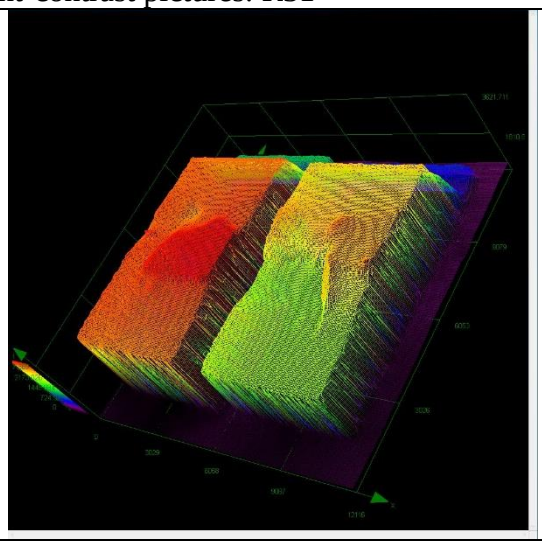

Optical microscopic and height-contrast pictures: R32

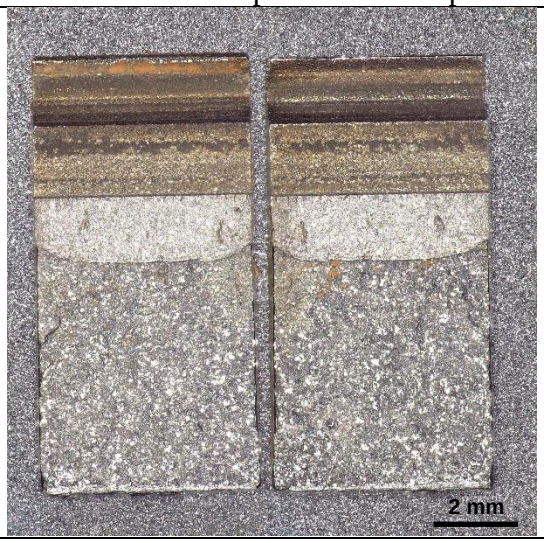

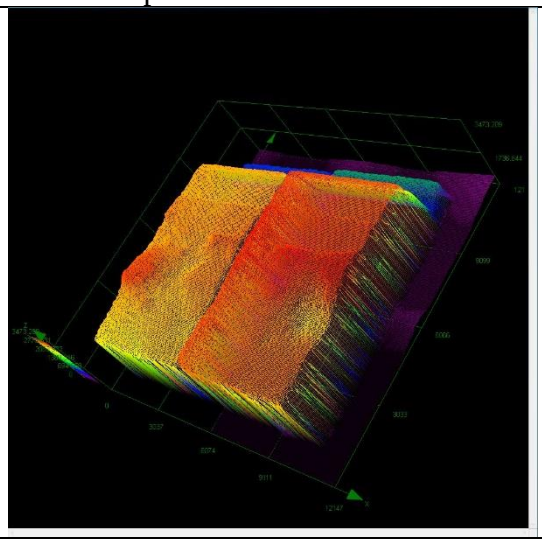

Optical microscopic and height-contrast pictures: R33

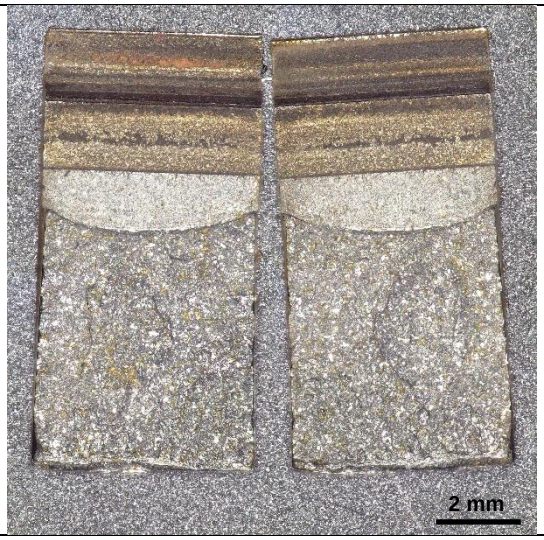

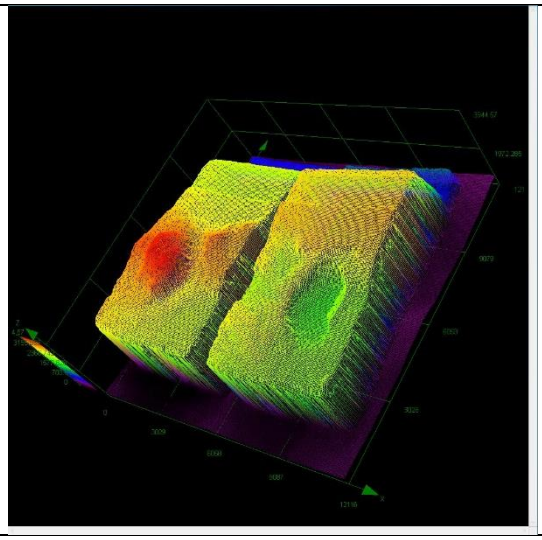

Optical microscopic and height-contrast pictures: R34

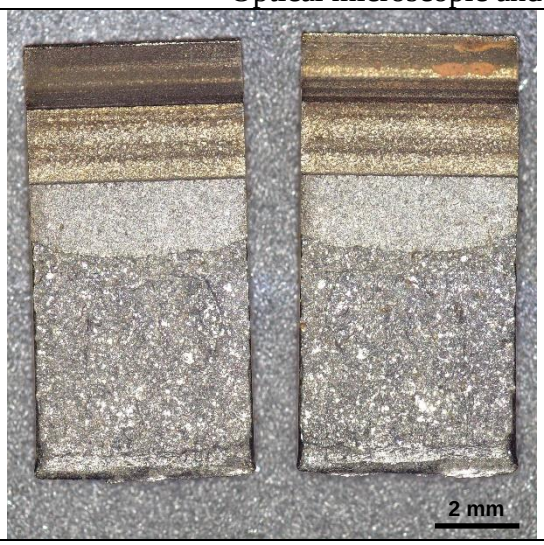

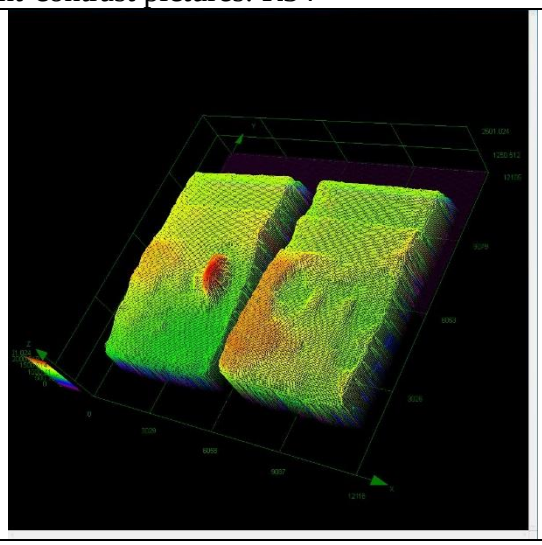

Optical microscopic and height-contrast pictures: R39

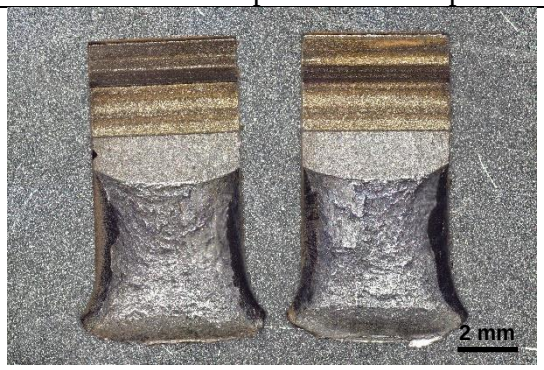

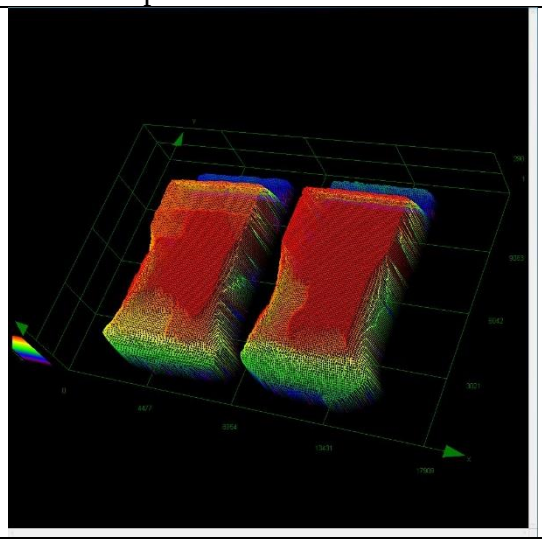

Optical microscopic and height-contrast pictures: R40